

# Chapter 4

## Spatiotemporal Pattern Formation in Neural Fields with Linear Adaptation

G. Bard Ermentrout, Stefanos E. Folias, and Zachary P. Kilpatrick

**Abstract** We study spatiotemporal patterns of activity that emerge in neural fields in the presence of linear adaptation. Using an amplitude equation approach, we show that bifurcations from the homogeneous rest state can lead to a wide variety of stationary and propagating patterns on one- and two-dimensional periodic domains, particularly in the case of lateral-inhibitory synaptic weights. Other typical solutions are stationary and traveling localized activity bumps; however, we observe exotic time-periodic localized patterns as well. Using linear stability analysis that perturbs about stationary and traveling bump solutions, we study conditions for the activity to lock to a stationary or traveling external input on both periodic and infinite one-dimensional spatial domains. Hopf and saddle-node bifurcations can signify the boundary beyond which stationary or traveling bumps fail to lock to external inputs. Just beyond a Hopf bifurcation point, activity bumps often begin to oscillate, becoming *breather* or *slosher* solutions.

### 4.1 Introduction

Neural fields that include local negative feedback have proven very useful in qualitatively describing the propagation of experimentally observed neural activity [26, 39]. Disinhibited in vitro cortical slices can support traveling pulses and spiral

---

G.B. Ermentrout (✉)  
Department of Mathematics, University of Pittsburgh, Pittsburgh, PA, USA  
e-mail: [bard@pitt.edu](mailto:bard@pitt.edu)

S.E. Folias  
Department of Mathematics & Statistics, University of Alaska Anchorage, Anchorage, AK, USA  
e-mail: [sfolias@uaa.alaska.edu](mailto:sfolias@uaa.alaska.edu)

Z.P. Kilpatrick  
Department of Mathematics, University of Houston, Houston, TX, USA  
e-mail: [zpkilpat@math.uh.edu](mailto:zpkilpat@math.uh.edu)

waves [27, 53], suggesting that some process other than inhibition must curtail large-scale neural excitations. A common candidate for this negative feedback is spike frequency adaptation, a cellular process that brings neurons back to their resting voltage after periods of high activity [2, 48]. Often, adaptation is modeled as an additional subtractive variable in the activity equation of a spatially extended neural field [26, 38, 39]. Pinto, in his PhD dissertation with Ermentrout, explored how linear adaptation leads to the formation of traveling pulses [38]. Both singular perturbation theory and the Heaviside formalism of Amari (see Chap. 3 and [1]) were used to analyze an excitatory network on the infinite spatial domain [38, 39]. At the same time, Hansel and Sompolinsky showed adaptation leads to traveling pulses (traveling bumps) in a neural field on the ring domain [26]. In the absence of adaptation, excitatory neural fields generate stable traveling fronts [21, 25]. For weak adaptation, the model still supports fronts which undergo a symmetry breaking bifurcation, leading to bidirectional front propagation at a critical value of the adaptation rate [6]. In fact, adaptive neural fields generate a rich variety of spatiotemporal dynamics like stimulus-induced breathers [7], spiral waves (see Chap. 5 and [27]), drifting spots (see Chap. 7), multipulse solutions [52], and self-sustained oscillations [46]. Coombes and Owen have implemented a related model, employing nonlinear adaptation, that is shown to generate breathers, traveling bumps, and more exotic solutions [11]. However, it has been shown that great care must be taken when performing stability analysis of such a model [29]. Thus, we restrict the contents of this chapter to analyzing models with linear adaptation.

We review a variety of results concerning bifurcations that arise in spatially extended neural fields when an auxiliary variable representing linear adaptation is included [13, 23, 25, 31]. In particular, we study the dynamics of the system of non-local integro-differential equations [10, 26, 35, 39]

$$\tau \frac{\partial u(x, t)}{\partial t} = -u(x, t) - \beta v(x, t) + \int_D w(x - y) F(u(y, t)) dy + I(x, t), \quad (4.1a)$$

$$\frac{1}{\alpha} \frac{\partial v(x, t)}{\partial t} = u(x, t) - v(x, t). \quad (4.1b)$$

The variable  $u(x, t)$  represents the total synaptic input arriving at location  $x \in D$  in the network at time  $t$ . We fix time units by setting  $\tau = 1$  without loss of generality. The convolution term represents the effects of recurrent synaptic interactions, and  $w(x - y) = w(y - x)$  is a reflection-symmetric, distance-dependent synaptic weight function encoding the strength of connections between location  $y$  and  $x$ . The nonlinearity  $F$  is a transfer function that converts the synaptic inputs to an output firing rate. Local negative feedback  $v(x, t)$  represents the effects of spike frequency adaptation [2, 26, 39, 48], occurring at rate  $\alpha$  with strength  $\beta$ . Finally,  $I(x, t)$  represents an external spatiotemporal input. In Sect. 4.2, we begin by analyzing bifurcations from the rest state on one- and two-dimensional periodic domains in the absence of any input ( $I(x, t) \equiv 0$ ) with the use of amplitude equations. We show that a lateral-inhibitory synaptic weight organizes activity of the network into

a wide variety of stationary and propagating spatiotemporal patterns. In Sect. 4.3, we study the processing of external inputs on a ring domain ( $D = (-\pi, \pi)$ ). Since adaptation can lead to spontaneous propagation of activity, inputs must move at a speed that is close to the natural wavespeed of the network to be well tracked by its activity. Finally, in Sect. 4.4, we study bifurcations of stationary and traveling bumps in a network on the infinite spatial domain ( $D = (-\infty, \infty)$ ). Both natural and stimulus-induced bump solutions are analyzed. Depending on whether the synaptic weight function is purely excitatory or lateral-inhibitory, either spatial mode of a stimulus-locked bump can destabilize in a Hopf bifurcation, leading to a *breather* or a *slosher*. Conditions for the locking of traveling bumps to moving inputs are discussed as well.

## 4.2 Bifurcations from the Homogeneous State

The simplest type of analysis that can be done with continuum neural field models is to study bifurcations from the homogeneous state. As in [13], we focus on the one-dimensional ring model, and then make some comments about the dynamics of systems in two space dimensions with periodic boundary conditions. Here, our domain is either the ring ( $D = (-\pi, \pi)$ ) or the square ( $D = (-\pi, \pi) \times (-\pi, \pi)$ ) with periodic boundary conditions. With some abuse of notation,  $x$  is either a scalar or a two-dimensional vector. The function  $w(x)$  is periodic in its coordinates and furthermore, we assume that it is symmetric in one-dimension and isotropic in two-dimensions. Translation invariance and periodicity assures us that  $\int_D w(x-y)dy = W_0$ . A constant steady state has the form

$$u(x, t) = \bar{u}, \quad \text{where} \quad (1 + \beta)\bar{u} = W_0 F(\bar{u}).$$

Since  $F$  is monotonically increasing with  $F(-\infty) = 0$  and  $F(+\infty) = 1$ , we are guaranteed at least one root. To simplify the analysis further, we assume that  $F(u) = k(f(u) - f(0))/f'(0)$  with  $f(u) = 1/(1 + \exp(-r(u - u_{th})))$  as in [13]. Note that  $F(0) = 0$  and  $F'(0) = k$  which serves as our bifurcation parameter. With this assumption,  $\bar{u} = \bar{v} = 0$  is the homogeneous rest state.

To study the stability, we linearize, letting  $u(x, t) = \bar{u} + q(x, t)$  and  $v(x, t) = \bar{v} + p(x, t)$  so that to linear order in  $q(x, t)$ ,  $p(x, t)$  we have

$$\begin{aligned} \frac{\partial q}{\partial t} &= -q(x, t) + k \int_{\Omega} w(x-y)q(y, t) dy - \beta p(x, t) \\ \frac{\partial p}{\partial t} &= \alpha(-p(x, t) + q(x, t)). \end{aligned} \quad (4.2)$$

Because  $w(x)$  is translational invariant and the domain is periodic, solutions to the linearized equations have the form  $\exp(\lambda t) \exp(in \cdot x)$  where in one-dimension  $n$  is

an integer and in two-dimensions, it is a pair of integers,  $(n_1, n_2)$ . Let  $m = |n|$  be the magnitude of this vector (scalar) and let

$$W(m) := \int_{\Omega} w(y) e^{-in \cdot y} dy.$$

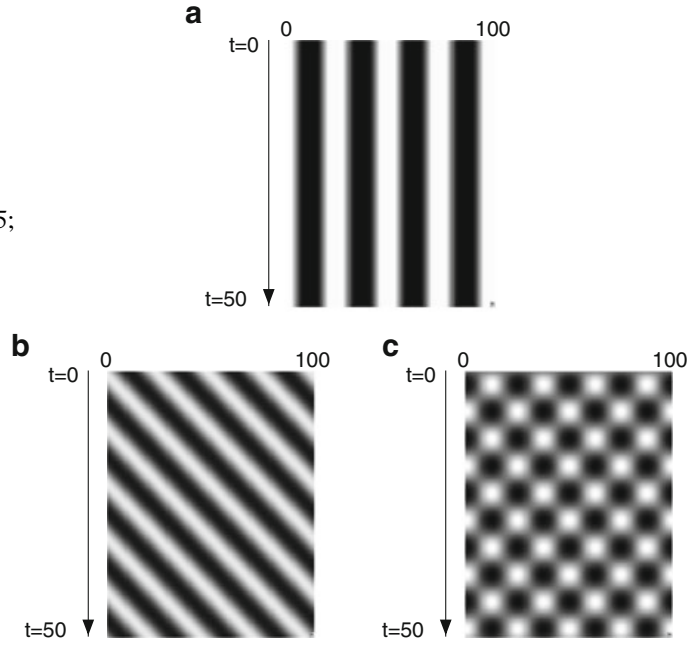
(The isotropy of  $w$  guarantees that the integral depends only on the magnitude of  $n$ .) We then see that  $\lambda$  must satisfy

$$\lambda \begin{pmatrix} \chi_1 \\ \chi_2 \end{pmatrix} = \begin{pmatrix} -1 + kW_m & -\beta \\ \alpha & -\alpha \end{pmatrix} \begin{pmatrix} \chi_1 \\ \chi_2 \end{pmatrix}, \quad (4.3)$$

where  $(\chi_1, \chi_2)^T$  is a constant eigenvector.

There are several cases with which to contend, and we now describe them. The easiest parameter to vary in this system is the sensitivity,  $k$  (This is the slope of  $F$  at the equilibrium point). The trace of this matrix is  $\mathcal{T}(m) := -(1 + \alpha) + kW(m)$  and the determinant is  $\mathcal{D}(m) := \alpha[1 + \beta - kW(m)]$ . Note that  $W(0) = W_0$  and  $W(m) \rightarrow 0$  as  $m \rightarrow \infty$ . The uniform state is linearly stable if and only if  $\mathcal{T}(m) < 0$  and  $\mathcal{D}(m) > 0$  for all  $m$ . If  $W(m) < 0$ , then both stability conditions hold, so, consider the sets  $k_m^{\mathcal{T}} = (1 + \alpha)/W(m)$  and  $k_m^{\mathcal{D}} = (1 + \beta)/W(m)$  which represent critical values of  $k$  where the trace and determinant vanish respectively. We are interested in the minimum of these sets over all values of  $m$  where  $W(m) > 0$ . Let  $n$  denote the critical wavenumber at which  $W(m)$  is maximal. It is clear that if  $\alpha > \beta$  then the determinant vanishes at a lower value of  $k$  than the trace does and *vice versa*. That is, there is a critical ratio  $R = \beta/\alpha$  such that if  $R > 1$ , then the trace is critical (and there is a Hopf bifurcation) while if  $R < 1$ , the determinant is critical (and there is a stationary bifurcation). The ratio  $R$  is the product of the strength and the time constant of the adaptation. If the adaptation is weak and fast, there is a steady state bifurcation, while if it is large and slow, there is a Hopf bifurcation. Curtu and Ermentrout [13] studied the special case where  $R$  is close to 1. At  $R = 1$ , there is a double zero eigenvalue at the critical wavenumber  $m$  and thus a Takens-Bogdanov bifurcation. For the rest of this section, let  $m^*$  denote the value of  $|n|$  at which  $W(m)$  is maximal. We also assume that  $W(m^*) > 0$ . For one dimension,  $n = \pm m^*$  and in two spatial dimensions, at criticality,  $n = (n_1, n_2)$  where  $m^* = \sqrt{n_1^2 + n_2^2}$ . For concreteness and illustration of the results, we use  $f(u) = 1/(1 + \exp(-r(u - u_{th})))$  with two free parameters that set the shape of  $f$  and thus  $F$ . We remark that (i) if  $u_{th} = 0$ , then  $F''(0) = 0$  and (ii) for a range of  $u_{th}$  surrounding 0,  $F'''(0) < 0$ . We also use  $w(x) = Aa^{p/2} \exp(-ax^2) - Bb^{p/2} \exp(-bx^2)$  (where  $p$  is the dimension of the domain) and note that  $W(m) = \pi(A \exp(-m^2/a) - B \exp(-m^2/b))$ . With  $A = 5, a = 0.125, B = 4, b = 0.005$ , this kernel has a fairly narrow Mexican hat profile.

**Fig. 4.1** Space-time plots of the solutions to (4.1). (a) Stationary stripes for  $k = 0.24$ ,  $\beta = 0$ ,  $\alpha = 0.1$ ,  $u_{th} = 0.05$ , and  $r = 0.25$ ; (b) Traveling waves with parameters as in (a), but  $\beta = 0.25$ ,  $k = 0.26$ ,  $u_{th} = 0.05$ ; (c) Standing waves with parameters as in A, B, but  $u_{th} = 0.3$



## 4.2.1 One Spatial Dimension

### 4.2.1.1 Zero Eigenvalue

In the case of  $R < 1$ , the bifurcation is at a zero eigenvalue and we expect a spatial pattern that has the form  $u(x, t) = z \exp(im^*x) + \text{c.c}$  (here c.c means complex conjugates) and

$$z_t = z(a(k - k_c) - b|z|^2)$$

where  $a$  and  $b$  are complicated, but readily computed, functions of  $w$ ,  $F''(0)^2$ , and  $F'''(0)$ . Both  $a, b$  are real,  $a > 0$ , and for our choice of  $w$  and  $F$ , we have  $b > 0$ . The non-zero solution to this equation is  $z = Ae^{-i\Theta}$  where  $A^2 = a(k - k_c)/b$  and  $\Theta$  is an arbitrary constant corresponding to a phase-shift of the periodic pattern. The solution exists as long as  $k \geq k_c$  (since  $a, b$  are positive) and, furthermore, the solution is stable. Thus as we increase  $k$ , we expect to see a spatially periodic pattern emerge that has the form

$$u(x) = \sqrt{a(k - k_c)/b} \cos(m^*x + \Theta) + O(k - k_c).$$

Figure 4.1a shows a simulation of Eq. (4.1) where we have discretized the one-dimensional ring into 100 units. In this case  $W(m)$  takes its maximum at  $m^* = 4$ , so as expected, we see a stationary pattern consisting of four peaks. In the case where  $m^* = 1$ , (which occurs for sufficiently broad inhibition) these spatially periodic patterns are interpreted as localized activity for tuning in a directionally based neural

system [26, 54]. This single stationary “bump” can be perturbed and pinned with external stimuli as we see in subsequent sections of this chapter.

#### 4.2.1.2 Imaginary Eigenvalues

When  $R > 1$  (strong or slow adaptation), then the trace vanishes at a lower critical  $k$  than the determinant. Let  $m^* > 0$  be the critical wavenumber and  $i\omega$  be the imaginary eigenvalue. Then  $u(x, t)$  has the form

$$u(x, t) = z(t)e^{i(\omega t - m^* x)} + w(t)e^{i(\omega t + m^* x)} + \text{c.c.}$$

where

$$\begin{aligned} z' &= z[(a_1 + ia_2)(k - k_c) - (b_1 + ib_2)|z|^2 - (c_1 + ic_2)|w|^2] \\ w' &= w[(a_1 + ia_2)(k - k_c) - (b_1 + ib_2)|w|^2 - (c_1 + ic_2)|z|^2]. \end{aligned} \quad (4.4)$$

These coefficients can be computed for (4.1) (and, indeed, for a variant of the equations, [13] computes them explicitly) and they depend only on  $F''(0)^2$ ,  $F'''(0)$ ,  $W(2m)$ ,  $W(m)$ ,  $\alpha$ , and  $\beta$ . In particular, with our choice of  $f(u)$  and for  $u_{th}$  not large,  $b_1, c_1 > 0$ . There are three distinct types of nontrivial solutions:  $(z, w) \in \{(Z, 0), (0, Z), (Y, Y)\}$ , where:

$$\begin{aligned} Z &= Ae^{i\Omega t}, & Y &= Be^{i\Xi t}, \\ \Omega &= (a_2 - a_1 b_2 / b_1)(k - k_c), & \Xi &= (a_2 - a_1(b_2 + c_2) / (b_1 + c_1))(k - k_c), \\ A^2 &= (a_1 / b_1)(k - k_c), & B^2 &= (a_1 / (b_1 + c_1))(k - k_c). \end{aligned}$$

Solutions of the form  $(Z, 0)$ ,  $(0, Z)$  correspond to traveling wavetrains with opposite velocities and those of the form  $(Y, Y)$  correspond to standing time-periodic waves. To see this, we note that the solutions have the form

$$u(x, t) = \Re\{ze^{i(\omega t + m^* x)} + we^{i(\omega t - m^* x)}\},$$

so that for the solution,  $(Z, 0)$ , we get

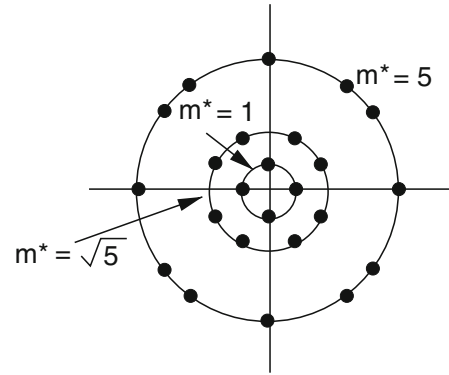
$$u(x, t) = A \cos((\omega + \Omega)t + m^* x),$$

while for the  $(Y, Y)$  case

$$u(x, t) = B \cos((\omega + \Xi)t) \cos(m^* x).$$

The traveling (standing) waves are stable if and only if  $c_1 > b_1$  (resp.  $c_1 < b_1$ ) and, importantly, if  $F''(0)$  is zero or close to zero (that is,  $u_{th} \approx 0$ ), then  $c_1 > b_1$  no matter what you choose for the other parameters. Thus, for  $u_{th}$  small, we expect to

**Fig. 4.2** Three different cases of critical wavenumbers in the square lattice. The critical wavenumbers are (from out to in),  $\{(\pm 1, 0), (0, \pm 1)\}$ ,  $\{(\pm 2, 1), (\pm 2, -1), (\pm 1, 2), (\pm 1, -2)\}$  and  $\{(\pm 3, 4), (\pm 3, -4), (\pm 4, 3), (\pm 4, -3), (\pm 5, 0), (0, \pm 5)\}$



see only stable traveling waves. Figure 4.1b, c shows simulations of (4.1) for two different choices of  $u_{th}$ ; near zero, the result is traveling waves, while for  $u_{th} = 0.3$ , standing waves emerge. Choosing the interaction kernel,  $w(x)$ , so that  $m^* = 1$ , leads to a single traveling pulse or bump of activity which, itself, can be entrained and perturbed by external stimuli (see the next sections).

## 4.2.2 Two Spatial Dimensions

While most of the focus in this chapter is on one space dimension, the theory of pattern formation is much richer in two-dimensions and Eq.(4.1) provides an excellent example of the variety of patterns. The isotropy of the weight matrix implies that the eigensolutions to the linear convolution equation (4.2) have the form  $\exp(in \cdot x)$ . In two dimensions,  $n$  is a two-vector of integers. We then obtain exactly the same formula for the determinant and the trace as in one-dimension, however,  $m = |n|$  in this case so that there are at least two distinct eigenvectors and their complex conjugates and there are often many more. Figure 4.2 illustrates three cases where  $m^* = 1, \sqrt{5}, 5$  corresponding to 4, 8, and 12 different pairs  $(n_1, n_2)$ . We treat and numerically illustrate several possibilities by discretizing (4.1) on a  $50 \times 50$  array. Our choice of  $w(x)$  gives a maximum at  $m^* = 2$  which is the simplest case.

### 4.2.2.1 Zero Eigenvalue

The simplest possible case in two dimensions has only four distinct wave vectors (inner circle in Fig.4.2). For example, if  $m^* = 2$ , then  $n \in \{(2, 0), (0, 2), (-2, 0), (0, -2)\}$ . (Note that in cases where there are only four vectors, the critical waves have either of the two forms:  $(k, 0), (0, k), (-k, 0), (0, -k)$  or  $(k, k), (k, -k), (-k, -k), (-k, k)$ .) If we write  $x = (x_1, x_2)$ , then,  $u(x, t)$  has the form  $u(x_1, x_2, t) = z_1 \exp(i2x_1) + z_2 \exp(i2x_2) + \text{c.c}$  and

$$\begin{aligned} z_1' &= z_1(a(k - k_c) - b|z_1|^2 - c|z_2|^2), \\ z_2' &= z_2(a(k - k_c) - b|z_2|^2 - c|z_1|^2), \end{aligned} \quad (4.5)$$

where as in the one-dimensional case,  $b, c$  depend on  $F''(0)^2, F'''(0)$ . All coefficients are real and can be computed. They are all positive for our choices of  $F(u)$ . We let  $z_j = A_j e^{i\theta_j}$  and we then find that

$$\begin{aligned} A_1' &= A_1(a(k - k_c) - bA_1^2 - cA_2^2), \\ A_2' &= A_2(a(k - k_c) - bA_2^2 - cA_1^2). \end{aligned}$$

It is an elementary calculation to show that there are three types of solutions,  $(z_1, z_2) = \{(r_1, 0), (0, r_1), (r_2, r_2)\}$  where  $r_1^2 = a(k - k_c)/b, r_2^2 = a(k - k_c)/(b + c)$ . For this example, the first two solutions correspond to vertical and horizontal stripes respectively and the third solution represents a spotted or checkerboard pattern. Stripes (spots) are stable if and only if  $b < c$  (resp.  $b > c$ ) [16]. As in the traveling/standing wave case above, if  $F''(0)$  is zero ( $u_{th} = 0$ ), then,  $c > b$  and there are only stable stripes [16]. The resulting stationary patterns look identical to those in Fig. 4.3a, b without the implied motion. (To get stationary patterns, choose, e.g.,  $\beta = 0, r = 3$ , and  $u_{th} = 0$  for stripes or  $u_{th} = 0.3$  for spots.)

This case (of two real amplitude equations) is the simplest case. The critical wave vector can be more complicated, for example, if  $m^* = \sqrt{5}$ , then,  $n \in \{(1, 2), (1, -2), (2, 1), (2, -1), (-1, -2), (-1, 2), (-2, -1), (-2, 1)\}$  for which there are eight eigenvectors and the solution has the form

$$u(x, t) = \sum_{j=1}^4 z_j(t) e^{in_j \cdot x} + \text{c.c.},$$

where  $n_j = (1, 2), \dots$  and  $z_j$  satisfy the four independent amplitude equations

$$\begin{aligned} z_1' &= z_1(a(k - k_c) - b|z_1|^2 - c|z_2|^2 - d|z_3|^2 - e|z_4|^2), \\ z_2' &= z_2(a(k - k_c) - b|z_2|^2 - c|z_1|^2 - d|z_4|^2 - e|z_3|^2), \\ z_3' &= z_3(a(k - k_c) - b|z_3|^2 - c|z_4|^2 - d|z_1|^2 - e|z_2|^2), \\ z_4' &= z_4(a(k - k_c) - b|z_4|^2 - c|z_3|^2 - d|z_2|^2 - e|z_1|^2). \end{aligned}$$

As in Eqs. (4.5), since  $a, \dots, e$  are all real coefficients, this model can be reduced to the analysis of a four dimensional real system. Dionne et al. [15] derive and analyze this case (among many others). In the context of neural fields, Tass [49] and Ermentrout [17] provide stability conditions for the equilibria, all of which consist of  $z_j$  taking on values of some  $A \neq 0$  or 0. For example, the pure patterns  $z_1 = A, z_2, z_3, z_4 = 0$  are stable if and only if  $a < \{b, c, d\}$ , there are also pairwise mixed solutions (checkerboards) of the form  $z_1 = z_2 = A', z_3 = z_4 = 0$ , etc., and fully

nonzero solutions,  $z_1 = z_2 = z_3 = z_4 = A''$  which are stable if  $a > \{d + c - b, d + b - c, b + c - d\}$ . We remark that the triplet solutions  $z_j = z_k = z_l = A'''$  are never stable and that if  $F''(0) = 0$ , then only stripes (one  $z_j$ , nonzero).

In two spatial dimensions,  $m^* = 1$  can correspond to a single bump of activity which has been used to model hippocampal place cells [28]. For narrower inhibition, the more complex patterns describe the onset of geometric visual hallucinations [5, 18, 49, 50]. Simple geometric hallucinations take the form of spirals, pinwheels, bullseyes, mosaics, and honeycombs [33]. When transformed from the retinocentric coordinates of the eyeball to the coordinates of the visual cortex, these patterns take the form of simple geometric planforms such as rolls, hexagons, squares, etc. [45]. Thus, spontaneous bifurcations to patterned activity form a natural model for the simple visual patterns seen when the visual system is perturbed by hallucinogens, flicker [43] or other excitation. (See [3] for a comprehensive review.)

#### 4.2.2.2 Imaginary Eigenvalues

The case of imaginary eigenvalues on a square lattice is quite complicated and only partially analyzed. Tass [50] has studied this case extensively when there are no even terms in the nonlinear equations (corresponding to  $u_t = 0$  in our model). Silber and Knobloch [47] provide a comprehensive and extremely readable analysis of case where there are four critical wavenumbers.

Let us first consider the four dimensional case and take as a specific example:  $n \in \{(2, 0), (0, 2), (-2, 0), (0, -2)\}$ . In this case, the firing rate has the form:

$$u(x, t) = z_1 e^{i2x_1 + i\omega t} + z_2 e^{i2x_2 + i\omega t} + z_3 e^{-i2x_1 + i\omega t} + z_4 e^{-i2x_2 + i\omega t} + \text{c.c.}$$

The complex amplitudes  $z_j$  satisfy normal form equations ([47], equation 5.3):

$$\begin{aligned} z_1' &= z_1[a(k - k_c) - b|z_1|^2 - cN_1 - dN_2] - e\bar{z}_3 z_2 z_4 & (4.6) \\ z_2' &= z_2[a(k - k_c) - b|z_2|^2 - cN_2 - dN_1] - e\bar{z}_4 z_1 z_3 \\ z_3' &= z_3[a(k - k_c) - b|z_3|^2 - cN_1 - dN_2] - e\bar{z}_1 z_2 z_4 \\ z_4' &= z_4[a(k - k_c) - b|z_4|^2 - cN_2 - dN_1] - e\bar{z}_2 z_1 z_3 \end{aligned}$$

where  $N_1 = |z_1|^2 + |z_3|^2$  and  $N_2 = |z_2|^2 + |z_4|^2$ . Here,  $a, \dots, e$  are all complex numbers;  $a$  depends only on the linearized equation, while  $b, \dots, e$  depend on  $F''(0)^2, F'''(0)$  and  $w(x)$ . For the case of no quadratic nonlinearities ( $u_t = 0$ ),  $b = c = d = e$ . There are many qualitatively different solutions to this system which correspond to interesting patterns. Silber and Knobloch [47] describe each of them as well as their conditions for stability. Travelling roll patterns (TR) consist of either horizontal or vertical traveling waves that are constant along one direction. They correspond to solutions to Eq. (4.6) where exactly one  $z_j \neq 0$ . Standing rolls correspond to  $z_1 = z_3 \neq 0, z_2 = z_4 = 0$ . (Note, the contrary case with  $z_1 = z_3 = 0$

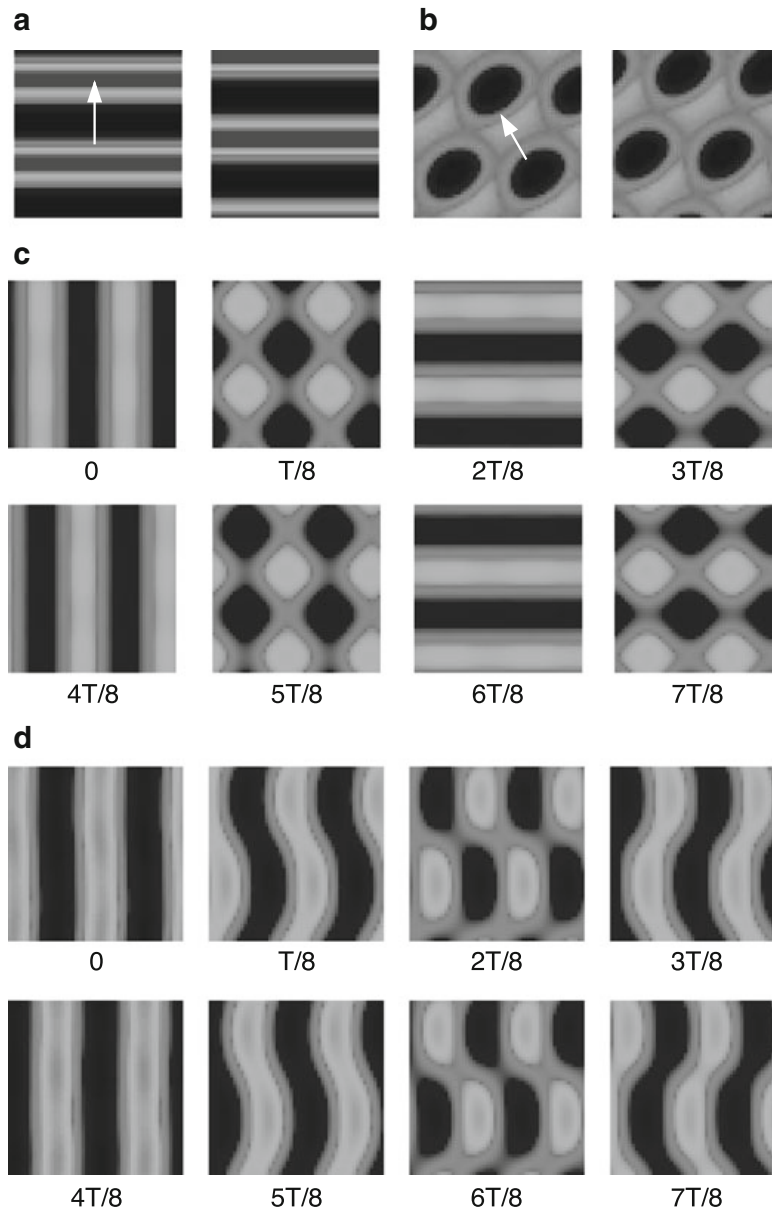


**Fig. 4.3** Two-dimensional time-periodic patterns with period  $T$  in (4.1) for  $\beta = 0.25, \alpha = 0.1$ : (a)  $k = 0.1, r = 3, u_{th} = 0$ ; (b)  $k = 0.09, r = 5, u_{th} = 0.3$ ; (c)  $k = 0.085, r = 3, u_{th} = 0$ ; (d)  $k = 0.09, r = 3, u_{th} = 0$

and  $z_2 = z_4 \neq 0$  are also standing rolls.) Traveling squares or spots correspond to  $z_1 = z_2 \neq 0$  and  $z_3 = z_4 = 0$ . Standing squares (a blinking checkerboard pattern) correspond to  $z_1 = z_2 = z_3 = z_4 \neq 0$ . A very interesting pattern that we see is the alternating roll pattern where horizontal blinking stripes switch to vertical blinking stripes. These correspond to solutions of the form  $z_1 = -iz_2 = z_3 = -iz_4 \neq 0$ . Figure 4.3 illustrates the results of simulations of Eq. (4.1) on the square doubly periodic domain in the case where  $m^* = 2$ . Thus, all the patterns show two spatial

cycles along the principle directions. In the simulations illustrated in the figure, we change  $u_{th}, r$  which affect the values of  $F''(0), F'''(0)$  and thus the values of the coefficients of the normal form, (4.6). The relative sizes of these coefficients determine both the amplitude and the stability of the patterns. Figure 4.3a shows the TR solutions for  $u_{th} = 0$  (which makes  $F''(0)$  vanish), while panel b shows a traveling spot pattern. Neither of these patterns can be simultaneously stable. However, there can be other patterns that stably coexist. Figure 4.3c illustrates the “alternating roll” pattern in which there is a switch from vertical to horizontal standing roles. Figure 4.3d shows a pattern that combines a standing roll (alternating vertical stripes) with a checkerboard pattern in between.

Dawes [14] has partially analyzed the more complicated case in which there are 8 critical wave vectors, for example  $m^* = \sqrt{5}$  in Fig. 4.2. All of the patterns we described above are also found as solutions to his amplitude equations. In some specific cases, he finds evidence of chaotic behavior. Thus, even near the bifurcation, we can expect the possibility of complex spatiotemporal dynamics in models like present equations. Tass [50] also considers this case, but only when the quadratic terms (e.g.,  $F''(0)$ ) are zero. Obviously, there is a great reduction in the complexity of the patterns and the resulting possibilities are restricted. The  $m^* = 5$  case has, to our knowledge, not yet been analyzed.

### 4.2.3 Summary of Pattern Formation

On a periodic one-dimensional domain, Eq. (4.1) can undergo a variety of bifurcations from the homogeneous state and these can be reduced via the construction of normal forms to one or two ordinary differential equations for the complex amplitudes. These bifurcations are generic in the sense that you can expect them to happen as you vary a *single* parameter. If you have the freedom to vary several parameters, then it is possible to arrange them so that multiple instabilities occur at the same time. For example [19] looked at the Wilson-Cowan neural field equations when  $W(m) = W(m+1)$  with corresponding imaginary eigenvalues (a double Hopf bifurcation). More recently, [13] studied (4.1) near  $R = 1$ . When  $R = 1$ , recall that both the trace and the determinant vanish at the critical wave number and critical sensitivity  $k$ . Thus, there is a Bogdanov-Takens bifurcation. The normal form is more complicated in this case; however for (4.1), the only solutions that were found were the stationary periodic patterns, standing waves, and traveling waves.

In two spatial dimensions, the dynamics is considerably richer due the symmetry of the square allowing for many critical wave vectors to become unstable simultaneously. The richness increases with the size of the critical wavenumber  $m^*$ . As a ballpark estimate, the critical wavenumber is proportional to the ratio of the domain size and the spatial scale of the connectivity function  $w(x)$ . Thus, for, say, global inhibition, the critical wavenumber is close to 1 and the possible patterns are very simple. We remark that by estimating the spatial frequency of visual hallucinations, it is possible to estimate the characteristic length scale in visual cortex [5].

### 4.3 Response to Inputs in the Ring Network

We now consider the effects of linear adaptation in the ring model [13, 26] in the presence of external inputs. We show that adaptation usually degrades the ability of the network to track input locations. We consider the domain  $D = (-\pi, \pi)$  and take  $w$  to be the cosine function [26]

$$w(x - y) = \cos(x - y), \quad (4.7)$$

so  $w(x - y) \geq 0$  when  $|x - y| \leq \pi/2$ . Networks with lateral-inhibitory synaptic weights like (4.7) are known to sustain stable stationary bumps [1, 4, 8, 26]. Many of our calculations are demonstrated in the case that the firing rate function  $f$  is the Heaviside step function (see Chaps. 3, 5, 7 and [1, 4, 8, 39]).

$$F(u) \equiv H(u - \theta) = \begin{cases} 1 & : x > \theta, \\ 0 & : x < \theta. \end{cases} \quad (4.8)$$

We consider both stationary and propagating inputs with the simple functional form

$$I(x, t) = I_0 \cos(x - c_0 t), \quad (4.9)$$

so they are unimodal in  $x$ . We study the variety of bifurcations that can arise in the system (4.1) due to the inclusion of adaptation and inputs.

For vanishing adaptation ( $\beta \rightarrow 0$ ), we find stable stationary bumps. For sufficiently strong adaptation, the input-free ( $I_0 = 0$ ) network (4.1) supports traveling bumps (pulses). The network locks to moving inputs as long as their speed is sufficiently close to that of naturally arising traveling bumps. Otherwise, activity periodically slips off of the stimulus or sloshes about the vicinity of the stimulus location. Previously, Hansel and Sompolinsky [26] studied many of these results, and recently [31] reinterpreted many of these findings in the context of hallucinogen-related visual pathologies.

#### 4.3.1 Existence of Stationary Bumps

First, we study existence of stationary bump solutions in the presence of stationary inputs ( $I(x, t) \equiv I(x)$ ). Assuming stationary solutions  $(u(x, t), v(x, t)) = (U(x), V(x))$  to (4.1) generates the single equation

$$(1 + \beta)U(x) = \int_{-\pi}^{\pi} w(x - y)F(U(y))dy + I(x). \quad (4.10)$$

For a cosine weight kernel (4.7), we can exploit the trigonometric identity

$$\cos(x - y) = \cos y \cos x + \sin y \sin x, \quad (4.11)$$

and consider the cosine input (4.9), which we take to be stationary ( $c_0 = 0$ ). This suggests looking for even-symmetric solutions

$$U(x) = \left( A + \frac{I_0}{1 + \beta} \right) \cos x, \quad (4.12)$$

so that the amplitude of (4.12) is specified by the implicit equation

$$A = \frac{1}{1 + \beta} \int_{-\pi}^{\pi} \cos y F((A + (1 + \beta)^{-1} I_0) \cos y) dy. \quad (4.13)$$

For a Heaviside firing rate function (4.8), we can simplify the implicit equation (4.13), using the fact that (4.12) is unimodal and symmetric so that  $U(x) > \theta$  for  $x \in (-a, a)$  for solutions  $A > 0$ . First of all, this means that the profile of  $U(x)$  crosses through threshold  $\theta$  at two distinct points [1, 4, 8]

$$U(\pm a) = [A + (1 + \beta)^{-1} I_0] \cos a = \theta \quad \Rightarrow \quad a = \cos^{-1} \left[ \frac{(1 + \beta)\theta}{(1 + \beta)A + I_0} \right]. \quad (4.14)$$

The threshold condition (4.14) converts the integral equation (4.13) to

$$A = \frac{1}{1 + \beta} \int_{-a}^a \cos y dy = \frac{2}{1 + \beta} \sqrt{1 - \frac{(1 + \beta)^2 \theta^2}{((1 + \beta)A + I_0)^2}}, \quad (4.15)$$

which can be converted to a quartic equation and solved analytically [30].

In the limit of no input  $I_0 \rightarrow 0$ , the amplitude of the bump is given by the pair of real roots of (4.15)

$$A_{\pm} = \frac{\sqrt{1 + (1 + \beta)\theta} \pm \sqrt{1 - (1 + \beta)\theta}}{1 + \beta}, \quad (4.16)$$

so there are two bump solutions. As is usually found in lateral inhibitory neural fields, the wide bump (+) is stable and the narrow bump (−) is unstable in the limit of vanishing adaptation ( $\beta \rightarrow 0$ ) [1, 4, 12, 40]. At a critical  $\beta$ , the wide bump undergoes a drift instability leading to a traveling bump.

### 4.3.2 Linear Stability of Stationary Bumps

We now compute stability of the bump (4.12) by studying the evolution of small, smooth, separable perturbations. By plugging  $u = U(x) + \psi(x)e^{\lambda t}$  and  $v = V(x) +$

$\phi(x)e^{\lambda t}$  (where  $|\psi(x)| \ll 1$  and  $|\phi(x)| \ll 1$ ) into (4.1), Taylor expanding, and truncating to first order we find the linear system

$$(\lambda + 1)\psi(x) = -\beta\phi(x) + \int_{-\pi}^{\pi} w(x-y)F'(U(y))\psi(y)dy, \quad (4.17)$$

$$(\lambda + \alpha)\phi(x) = \alpha\psi(x). \quad (4.18)$$

For the cosine weight function (4.7), we apply the identity (4.11) and substitute (4.18) into (4.17) to yield the single equation

$$\mathcal{Q}(\lambda)\psi(x) = (\lambda + \alpha)(\mathcal{A} \cos x + \mathcal{B} \sin x) \quad (4.19)$$

where  $\mathcal{Q}(\lambda) = (\lambda + \alpha)(\lambda + 1) + \alpha\beta$  and

$$\mathcal{A} = \int_{-\pi}^{\pi} \cos x F'(U(x))\psi(x)dx, \quad \mathcal{B} = \int_{-\pi}^{\pi} \sin x F'(U(x))\psi(x)dx. \quad (4.20)$$

We can then plug (4.19) into the system of equations (4.20) and simplify to yield

$$\mathcal{Q}(\lambda)\mathcal{A} = (\lambda + \alpha) \left( \int_{-\pi}^{\pi} F'(U(x))dx - \frac{(1 + \beta)^2 A}{(1 + \beta)A + I_0} \right) \mathcal{A}, \quad (4.21)$$

$$\mathcal{Q}(\lambda)\mathcal{B} = \frac{(\lambda + \alpha)(1 + \beta)^2 A}{(1 + \beta)A + I_0} \mathcal{B}, \quad (4.22)$$

where we have used the fact that integrating (4.13) by parts yields

$$A = \frac{A + (1 + \beta)^{-1} I_0}{1 + \beta} \int_{-\pi}^{\pi} \sin^2 x F'((A + (1 + \beta)^{-1} I_0) \cos x) dx,$$

as well as the fact that the off-diagonal terms vanish, since their integrands are odd. This means that the eigenvalues determining the linear stability of the bump (4.12) are of two classes: (a) those of even perturbations so  $\psi(x) = \cos x$  and (b) those of odd perturbations where  $\psi(x) = \sin x$ . We primarily study eigenvalues associated with odd perturbations, given by the quadratic equation

$$\lambda^2 + [1 + \alpha - (1 + \beta)\Omega]\lambda + \alpha(1 + \beta)(1 - \Omega) = 0, \quad \Omega = \frac{(1 + \beta)A}{(1 + \beta)A + I_0}. \quad (4.23)$$

We can use (4.23) to study two bifurcations of stationary bumps in the system (4.1). First, we show a drift instability arises in the input-free ( $I_0 = 0$ ) network, leading to a pitchfork bifurcation whose resultant attracting solutions are traveling bumps [10, 13, 26, 35, 39]. Second, we show that in the input-driven system ( $I_0 > 0$ ), an

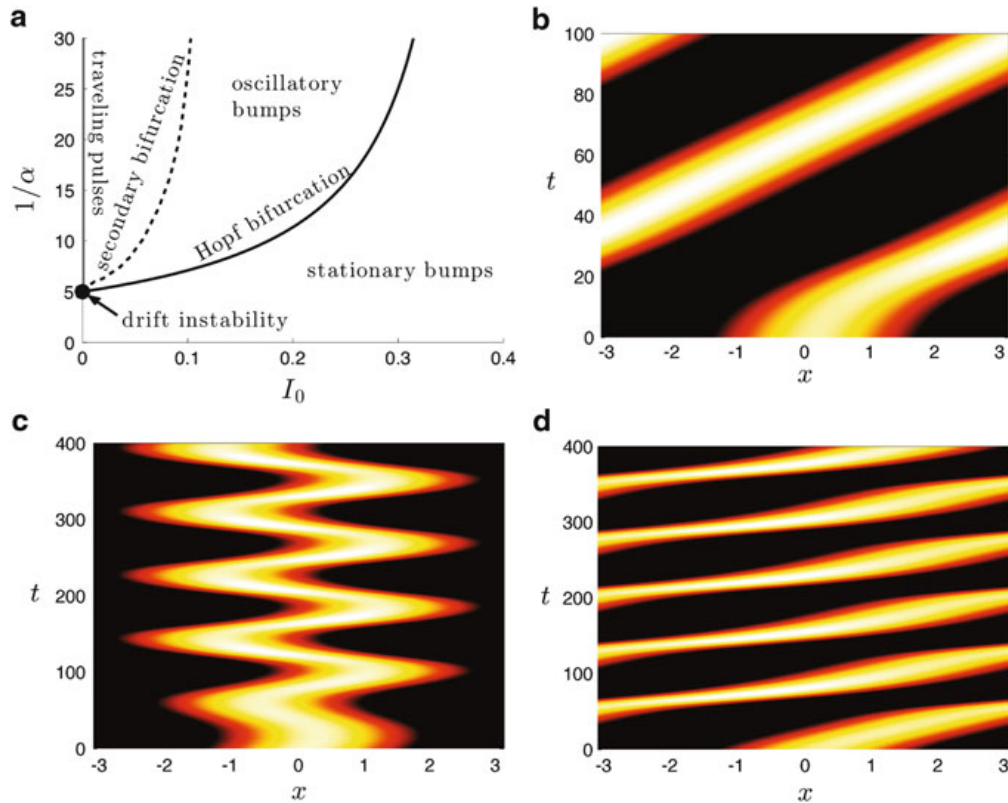


**Fig. 4.4** (a) Partition of  $(I_0, \alpha^{-1})$  parameter space into different dynamical behaviors of the bump solution (4.12) for Heaviside firing rate (4.8). Numerical simulation of the (b) drift instability of the bump (4.12) in the case of no input ( $I_0 = 0$ ); (c) sloshing oscillatory instability in the case of input  $I_0 = 0.1$ ; and (d) translation variant propagation in the case of weak input  $I_0 = 0.05$ . Other parameters are  $\theta = 0.5$ ,  $\alpha = 0.1$ , and  $\beta = 0.2$

oscillatory instability arises where the edges of the “slosh” periodically. This is a Hopf bifurcation, which also persists for moving inputs ( $c_0 > 0$ ).

In the limit of no input ( $I_0 \rightarrow 0$ ),  $\Omega \rightarrow 1$ , so (4.23) reduces to

$$\lambda^2 + [\alpha - \beta]\lambda = 0. \quad (4.24)$$

There is always a zero eigenvalue, due to the translation symmetry of the input-free network [1, 40]. Fixing adaptation strength  $\beta$ , we can decrease the rate  $\alpha$  from infinity to find the other eigenvalue crosses zero when  $\alpha = \beta$ . We mark this point in our partition of parameter space into different dynamical behaviors in Fig. 4.4a. This non-oscillatory instability results in a traveling bump, indicated by the associated shift eigenfunction ( $\sin x$ ). Traveling pulses can propagate in either direction, so the full system (4.1) undergoes a pitchfork bifurcation. We demonstrate the instability resulting in a traveling bump in Fig. 4.4b.

We could also ensure that instabilities associated with even perturbations ( $\cos x$ ) of the bump (4.12) do not occur prior to this loss of instability of the odd

perturbation. For brevity, we omit this calculation. Numerical simulations (as shown in Fig. 4.4b) verify odd perturbations are the first to destabilize. Therefore, we would always expect that as  $\alpha$  is decreased from infinity, the first instability that arises is associated with odd perturbations of the bump, leading to a drift instability and thus a traveling bump solution (see Fig. 4.4).

For nonzero input ( $I_0 > 0$ ), the primary bifurcation of the stable (wide) stationary bump solution is shown to be oscillatory. To identify the location of this Hopf bifurcation, we plug the ansatz  $\lambda = i\omega$  into (4.23) to find

$$-\omega^2 + i[(1 + \alpha) - (1 + \beta)\Omega]\lambda + \alpha(1 + \beta)(1 - \Omega) = 0. \quad (4.25)$$

Equating real and imaginary parts of (4.25), we find a Hopf bifurcation occurs when

$$\alpha_H = (1 + \beta)\Omega - 1, \quad (4.26)$$

with onset frequency

$$\omega_H = \sqrt{\alpha(1 + \beta)(1 - \Omega)}. \quad (4.27)$$

Since  $\Omega \in (0, 1)$  when  $I_0 > 0$ , we know that  $\omega_H > 0$  for all parameter values we consider. Therefore, there is never an instability with purely real eigenvalues associated with odd perturbations, in the case of nonzero input. We show the curve of Hopf bifurcations in  $(I_0, \alpha^{-1})$  parameter space in Fig. 4.4a as well as a simulation of the resulting oscillatory solution in Fig. 4.4c. Studies of input-driven excitatory networks reveal it is the even mode that destabilizes into oscillations, yielding reflection symmetric breathers [22, 23]. Here, due to the lateral inhibitory kernel, the odd eigenmode destabilizes, leading to sloshing breathers [22, 42]. As in the case of the drift instability, we should ensure that instabilities associated with even perturbations do not arise prior to the Hopf bifurcation. We have ensured this for the calculations of Fig. 4.4 but do not show this explicitly here.

Finally, we note a secondary bifurcation which leads to dynamics that evolves as a propagating pattern with varying width (see Fig. 4.4d). Essentially, the ‘‘sloshing’’ bump breaks free from the attraction of the pinning stimulus and begins to propagate. As it passes over the location of the stimulus, it expands. Such secondary bifurcations have been observed in adaptive neural fields on infinite spatial domains too [23]. While we cannot develop a linear theory for this bifurcation, we can determine the location of this bifurcation numerically.

### 4.3.3 Existence of Traveling Bumps

Our linear stability analysis of stationary bumps predicts the existence of traveling bumps for substantially slow and strong adaptation. We can also show that when

a moving input is introduced, the system tends to lock to it if it has speed commensurate with that of the natural wave. Converting to a wave coordinate frame  $\xi = x - c_0 t$  where we choose the stimulus speed  $c_0$ , we can study traveling wave solutions  $(u(x, t), v(x, t)) = (U(\xi), V(\xi))$  of (4.1) with the second order differential equation [23]

$$-c_0^2 U''(\xi) + c_0(1 + \alpha)U'(\xi) - \alpha(1 + \beta)U(\xi) = G(\xi) \quad (4.28)$$

where

$$G(\xi) = \left( c \frac{d}{d\xi} - \alpha \right) \left[ \int_{-\pi}^{\pi} w(\xi - y) F(U(y)) dy + I(\xi + \Delta_I) \right], \quad (4.29)$$

and  $\Delta_I$  specifies the spatial shift between the moving input and the pulse that tracks it. In the case of a cosine weight kernel (4.7) and input (4.9), we can apply the identity (4.11)–(4.29) so we may write Eq. (4.28) as

$$-c_0^2 U''(\xi) + c_0(1 + \alpha)U'(\xi) - \alpha(1 + \beta)U(\xi) = \mathcal{C} \cos \xi + \mathcal{S} \sin \xi. \quad (4.30)$$

where

$$\mathcal{C} = \int_{-\pi}^{\pi} \cos x [c_0 F'(U(x))U'(x) - \alpha F(U(x))] dx - I_0(\alpha \cos \Delta_I + c_0 \sin \Delta_I), \quad (4.31)$$

$$\mathcal{S} = \int_{-\pi}^{\pi} \sin x [c_0 F'(U(x))U'(x) - \alpha F(U(x))] dx + I_0(\alpha \sin \Delta_I - c_0 \cos \Delta_I). \quad (4.32)$$

By treating  $\mathcal{C}$  and  $\mathcal{S}$  as constants, it is straightforward to solve the second order differential equation (4.30) to find

$$U(\xi) = \frac{(c_0^2 - \alpha - \alpha\beta)[\mathcal{C} \cos \xi + \mathcal{S} \sin \xi] + c_0(1 + \alpha)[\mathcal{C} \sin \xi - \mathcal{S} \cos \xi]}{(c_0^2 - \alpha(1 + \beta))^2 + c_0^2(1 + \alpha)^2}. \quad (4.33)$$

In the case of a Heaviside firing rate function (4.8), we can evaluate the integral terms of  $\mathcal{C}$  and  $\mathcal{S}$  directly. First, we break the translation symmetry of the system by fixing the threshold crossing points,  $U(\pi) = U(\pi - \Delta) = \theta$ . This specifies the input shift parameter  $\Delta_I$  as well. We also require that the superthreshold region  $U(\xi) > \theta$  when  $x \in (\pi - \Delta, \pi)$  and  $U(\xi) < \theta$  otherwise. This yields

$$\mathcal{C} = \alpha \sin \Delta + c_0(1 - \cos \Delta) - I_0(\alpha \cos \Delta_I + c_0 \sin \Delta_I), \quad (4.34)$$

$$\mathcal{S} = c_0 \sin \Delta - \alpha(1 - \cos \Delta) + I_0(\alpha \sin \Delta_I - c_0 \cos \Delta_I). \quad (4.35)$$

Plugging this into (4.33) and imposing threshold conditions, we have the system

$$\frac{\mathcal{X}_1[\sin \Delta - I_0 \cos \Delta_I] - \mathcal{X}_2[1 - \cos \Delta - I_0 \sin \Delta_I]}{(c_0^2 - \alpha(1 + \beta))^2 + c_0^2(1 + \alpha)^2} = \theta, \quad (4.36)$$

$$\frac{\mathcal{X}_1[\sin \Delta - I_0 \cos(\Delta - \Delta_I)] + \mathcal{X}_2[1 - \cos \Delta - I_0 \sin(\Delta - \Delta_I)]}{(c_0^2 - \alpha(1 + \beta))^2 + c_0^2(1 + \alpha)^2} = \theta, \quad (4.37)$$

where  $\mathcal{X}_1 = c_0^2 + \alpha^2(1 + \beta)$  and  $\mathcal{X}_2 = c_0^3 + c_0\alpha^2 - c_0\alpha\beta$ , which we could solve the numerically (see [31]).

In the limit of no input ( $I_0 \rightarrow 0$ ), we can treat  $c = c_0$  as an unknown parameter. By taking the difference of (4.37) and (4.36) in this limit, we see that we can compute the speed of natural waves by studying solutions of

$$c^3 + c\alpha^2 - c\alpha\beta = 0, \quad (4.38)$$

a cubic equation providing up to three possible speeds for a traveling bump solution. The trivial  $c = 0$  solution is the limiting case of stationary bump solutions that we have already studied and is unstable when  $\alpha < \beta$ . In line with our bump stability predictions, for  $\alpha \leq \beta$ , we have the two additional solutions  $c_{\pm} = \pm\sqrt{\alpha\beta - \alpha^2}$ , which provides a right-moving (+) and left-moving (−) traveling bump solution. The pulse widths are then given applying the expression (4.38) into (4.36) and (4.37) and taking their mean to find  $\sin \Delta = (1 + \alpha)\theta$ . Thus, we can expect to find four traveling bump solutions, two with each speed, that have widths  $\Delta_s = \pi - \sin^{-1}[\theta(1 + \alpha)]$  and  $\Delta_u = \sin^{-1}[\theta(1 + \alpha)]$ . We can find, using linear stability analysis, that the two traveling bumps associated with the width  $\Delta_s$  are stable [35, 39].

#### 4.3.4 Linear Stability of Traveling Bumps

To analyze the linear stability of stimulus-locked traveling bumps (4.33), we study the evolution of small, smooth, separable perturbations to  $(U(\xi), V(\xi))$ . To find this, we plug the expansions  $u(x, t) = U(\xi) + \psi(\xi)e^{\lambda t}$  and  $v(x, t) = V(\xi) + \phi(\xi)e^{\lambda t}$  (where  $|\psi(\xi)| \ll 1$  and  $|\phi(\xi)| \ll 1$ ) and truncate to first order to find the linear equation [10, 25, 56]

$$-c_0\psi'(\xi) + (\lambda + 1)\psi(\xi) = -\beta\phi(\xi) + \int_{-\pi}^{\pi} w(\xi - y)F'(U(y))\psi(y)dy, \quad (4.39)$$

$$-c_0\phi'(\xi) + (\lambda + \alpha)\phi(\xi) = \alpha\psi(\xi). \quad (4.40)$$

For the cosine weight function (4.7), we can apply the identity (4.11), so that upon converting the system to a second order differential equation, we

$$-c_0^2\psi'' + c(2\lambda + 1 + \alpha)\psi' - [(\lambda + 1)(\lambda + \alpha) + \alpha\beta]\psi = \mathcal{A} \cos \xi + \mathcal{B} \sin \xi, \quad (4.41)$$

where

$$\mathcal{A} = -(\lambda + \alpha) \int_{-\pi}^{\pi} \cos \xi F'(U(\xi)) \psi(\xi) d\xi + c_0 \int_{-\pi}^{\pi} \sin \xi F'(U(\xi)) \psi(\xi) d\xi, \quad (4.42)$$

$$\mathcal{B} = -c_0 \int_{-\pi}^{\pi} \cos \xi F'(U(\xi)) \psi(\xi) d\xi - (\lambda + \alpha) \int_{-\pi}^{\pi} \sin \xi F'(U(\xi)) \psi(\xi) d\xi. \quad (4.43)$$

Employing periodic boundary conditions  $\psi(-\pi) = \psi(\pi)$  and  $\psi'(-\pi) = \psi'(\pi)$  and treating  $\mathcal{A}$  and  $\mathcal{B}$  as constants, it is then straightforward to solve (4.41) to find

$$\psi(\xi) = \frac{\mathcal{P}_2 \mathcal{A} - \mathcal{P}_1 \mathcal{B}}{\mathcal{D}_p} \cos \xi + \frac{\mathcal{P}_1 \mathcal{A} + \mathcal{P}_2 \mathcal{B}}{\mathcal{D}_p} \sin \xi. \quad (4.44)$$

where  $\mathcal{P}_1 = c_0(2\lambda + 1 + \alpha)$ ,  $\mathcal{P}_2 = c_0^2 - [(\lambda + 1)(\lambda + \alpha) + \alpha\beta]$ , and  $\mathcal{D}_p = \mathcal{P}_1^2 + \mathcal{P}_2^2$ . We can then use self-consistency to determine the constants  $\mathcal{A}$  and  $\mathcal{B}$ , which implicitly depend upon  $\psi$  itself. In the case that the firing rate function is a Heaviside (4.8), we can reduce this to a pointwise dependence, so that

$$\mathcal{A} = \frac{c_0 \sin \Delta \psi(\pi - \Delta)}{|U'(\pi - \Delta)|} + (\lambda + \alpha) \left[ \frac{\psi(\pi)}{|U'(\pi)|} + \frac{\cos \Delta \psi(\pi - \Delta)}{|U'(\pi - \Delta)|} \right], \quad (4.45)$$

$$\mathcal{B} = c_0 \left[ \frac{\psi(\pi)}{|U'(\pi)|} + \frac{\cos \Delta \psi(\pi - \Delta)}{|U'(\pi - \Delta)|} \right] - \frac{(\lambda + \alpha) \sin \Delta \psi(\pi - \Delta)}{|U'(\pi - \Delta)|}, \quad (4.46)$$

and we can write the solution

$$\psi(\xi) = \frac{\mathcal{C}_1 \cos \xi + \mathcal{S}_1 \sin \xi}{\mathcal{D}_p} \frac{\psi(\pi)}{|U'(\pi)|} + \frac{\mathcal{C}_2 \cos \xi + \mathcal{S}_2 \sin \xi}{\mathcal{D}_p} \frac{\psi(\pi - \Delta)}{|U'(\pi - \Delta)|},$$

where

$$\mathcal{C}_1 = \mathcal{P}_2(\lambda + \alpha) - \mathcal{P}_1 c_0, \quad \mathcal{S}_1 = \mathcal{P}_1(\lambda + \alpha) + \mathcal{P}_2 c_0,$$

$$\mathcal{C}_2 = \mathcal{P}_1((\lambda + \alpha) \sin \Delta - c_0 \cos \Delta) + \mathcal{P}_2(c_0 \sin \Delta + (\lambda + \alpha) \cos \Delta),$$

$$\mathcal{S}_2 = \mathcal{P}_1((\lambda + \alpha) \cos \Delta + c_0 \sin \Delta) + \mathcal{P}_2(c_0 \cos \Delta - (\lambda + \alpha) \sin \Delta).$$

Applying self consistency, we have a  $2 \times 2$  eigenvalue problem  $\Psi = \mathcal{A}_p \Psi$ , where

$$\Psi = \begin{pmatrix} \psi(\pi) \\ \psi(\pi - \Delta) \end{pmatrix}, \quad \mathcal{A}_p = \begin{pmatrix} \mathcal{A}_{\pi\pi} & \mathcal{A}_{\pi\Delta} \\ \mathcal{A}_{\Delta\pi} & \mathcal{A}_{\Delta\Delta} \end{pmatrix}, \quad (4.47)$$

with

$$\mathcal{A}_{\pi\pi} = -\frac{\mathcal{C}_1}{\mathcal{D}_p |U'(\pi)|}, \quad \mathcal{A}_{\pi\Delta} = -\frac{\mathcal{C}_2}{\mathcal{D}_p |U'(\pi - \Delta)|},$$

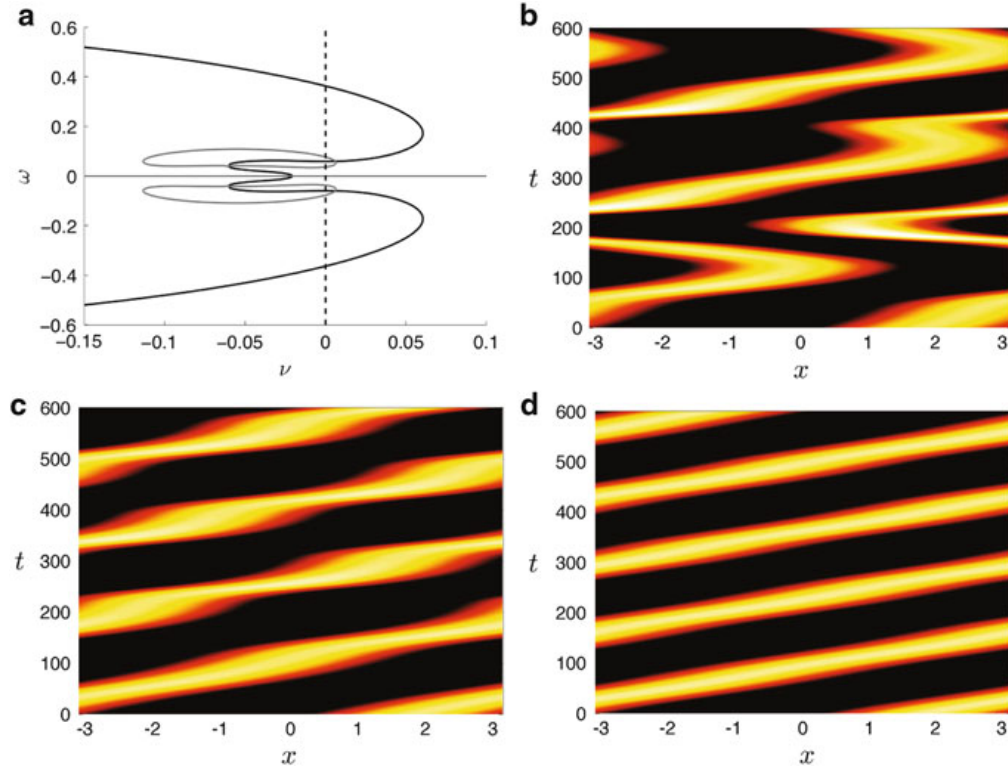


**Fig. 4.5** Slushing instability of stimulus-locked traveling bumps (4.33) in adaptive neural field (4.1) with Heaviside firing rate (4.8). (a) Dependence of stimulus locked pulse width  $\Delta$  on stimulus speed  $c_0$ , calculated using the implicit equations (4.36) and (4.37). (a) Zeros of the Evans function  $\mathcal{E}(\lambda) = \det(\mathcal{A}_p - I)$ , with (4.47), occur at the crossings of the zero contours of  $\text{Re}\mathcal{E}(\lambda)$  (black) and  $\text{Im}\mathcal{E}(\lambda)$  (grey). Presented here for stimulus speed  $c_0 = 0.042$ , just beyond the Hopf bifurcation at  $c_H \approx 0.046$ . Breathing instability occurs in numerical simulations for (b)  $c_0 = 0.036$  and (c)  $c_0 = 0.042$ . (d) When stimulus speed  $c_0 = 0.047$  is sufficiently fast, stable traveling bumps lock. Other parameters are  $\theta = 0.5$ ,  $\alpha = 0.05$ ,  $\beta = 0.2$ , and  $I_0 = 0.1$

$$\mathcal{A}_{\Delta\pi} = \frac{\mathcal{S}_1 \sin \Delta - \mathcal{C}_1 \cos \Delta}{\mathcal{D}_p |U'(\pi)|}, \quad \mathcal{A}_{\Delta\Delta} = \frac{\mathcal{S}_2 \sin \Delta - \mathcal{C}_2 \cos \Delta}{\mathcal{D}_p |U'(\pi - \Delta)|}.$$

Then, applying the approach of previous stability analyses of traveling waves in neural fields [10, 25, 56], we examine nontrivial solutions of  $\Psi = \mathcal{A}_p \Psi$  so that  $\mathcal{E}(\lambda) = 0$ , where  $\mathcal{E}(\lambda) = \det(\mathcal{A}_p - I)$  is called the Evans function of the traveling bump solution (4.33). Since no other parts of the spectrum contribute to instabilities in this case, the traveling bump is linearly stable as long as  $\text{Re } \lambda < 0$  for all  $\lambda$  such that  $\mathcal{E}(\lambda) = 0$ . We can find the zeros of the Evans function by following the approach of [10, 25] and writing  $\lambda = \nu + i\omega$  and plotting the zero contours of  $\text{Re } \mathcal{E}(\lambda)$  and  $\text{Im } \mathcal{E}(\lambda)$  in the  $(\nu, \omega)$ -plane. The Evans function is zero where the lines intersect.

We present examples of this analysis in Fig. 4.5. As shown, we can use the implicit equations (4.36) and (4.37) to compute the width of a stimulus-locked pulse as it depends upon the speed of the input in the case of a Heaviside firing rate

function (4.8). In parameter regime we show, there are two pulses for each parameter value, either both are unstable or one is stable. As the speed of stimuli is decreased, a stable traveling bump undergoes a Hopf bifurcation. For sufficiently fast stimuli, a stable traveling bump can lock to the stimulus, as shown in Fig. 4.5d. However, for sufficiently, slow stimuli, the speed of natural traveling bumps of the stimulus free network is too fast to track the stimuli. Therefore, an oscillatory instability results. We plot the zeros of the Evans functions associated with this instability in Fig. 4.5a. The sloshing pulses that result are pictured in Fig. 4.5b, c. Note that, as was shown in [31], it is possible for pulses to destabilize due to stimuli being too fast. In this context, such an instability occurs through a saddle-node bifurcation, rather than a Hopf.

## 4.4 Activity Bumps on the Infinite Line

We consider neural field (4.1) with a Heaviside firing rate function  $F(u) = H(u - \theta)$  with firing threshold  $\theta$  where  $u(x, t)$  and  $v(x, t)$  are defined along the infinite line with  $u(x, t), v(x, t) \rightarrow 0$  as  $x \rightarrow \pm\infty$ . The even-symmetric synaptic weight function  $w$  is assumed to be either excitatory ( $w(x) > 0$ ) or of Mexican hat form (locally positive, laterally negative) satisfying  $\int_{-\infty}^{\infty} w(y) dy < \infty$ . We consider *stationary* activity bumps in Sect. 4.4.1 and *traveling* activity bumps in Sect. 4.4.2 and examine the cases of (i) bumps generated intrinsically by the network with no input ( $I(x, t) = 0$ ) and (ii) bumps induced by a localized, excitatory input inhomogeneity ( $I(x, t) > 0$ ) which can be either stationary ( $I(x)$ ) or traveling ( $I(x - ct)$ ) with constant speed  $c$ . The input is assumed to have an even-symmetric, Gaussian-like profile satisfying  $I(x) \rightarrow 0$  as  $x \rightarrow \pm\infty$ .

### 4.4.1 Natural and Stimulus-Induced Stationary Activity Bumps

**Existence of Stationary Bumps.** An equilibrium solution of (4.1) is expressed as  $(u(x, t), v(x, t))^T = (U_o(x), V_o(x))^T$  and satisfies  $V_o(x) = U_o(x)$  and

$$(1 + \beta)U_o(x) = \int_{-\infty}^{\infty} w(x - y) H(U_o(y) - \theta) dy + I(x). \quad (4.48)$$

We follow the approach of Amari [1] to use the Heaviside firing rate and make the ansatz of an even-symmetric stationary bump  $U_o(x)$  that is centered about  $x = 0$ , is superthreshold  $U_o(x) > \theta$  for  $x \in (-a, a)$ , satisfies  $U_o(\pm a) = \theta$ , and is subthreshold otherwise with  $U_o(x) \rightarrow 0$  as  $x \rightarrow \pm\infty$  (see Fig. 4.6). That the stationary bump is centered about  $x = 0$  is by choice both (i) in the case of no input ( $I(x) = 0$ ) due to translation symmetry of the bump and (ii) in the presence

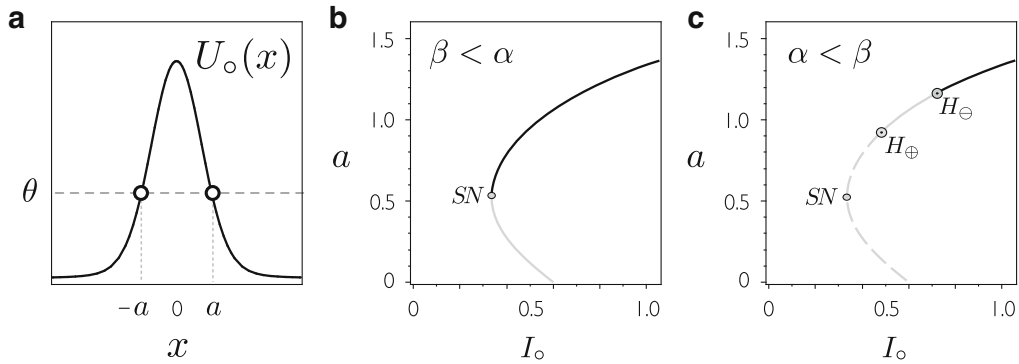


**Fig. 4.6** (a) Stationary bump profile  $U_o(x)$  with halfwidth  $a$ . Bifurcation curves satisfying (4.50) and illustrating the dependence of  $a$  on the bifurcation parameter  $I_o$  are shown in (b) for  $\beta < \alpha$  and in (c) for  $\alpha < \beta$ . Black (gray) denote stability (instability) of the stationary bump. SN denotes a saddle-node bifurcation and  $H_\oplus$  and  $H_\ominus$  denote Hopf bifurcations with respect to the sum mode  $\Omega_+$  and difference mode  $\Omega_-$ , respectively. Parameters are  $\bar{w}_e = 1$ ,  $\sigma_e = 1$ ,  $\bar{w}_i = 0.4$ ,  $\sigma_i = 2$ ,  $\theta = 0.3$ ,  $\alpha = 0.025$ ,  $\beta = 1$ ,  $\sigma = 1.2$  (Figure adapted from Folias [22])

of a stationary input ( $I(x) \neq 0$ ) where the stationary bump and the input share the same center, which is set to be  $x = 0$ . The profile  $U_o(x)$  of the stationary bump can then be expressed as

$$(1 + \beta)U_o(x) = \int_{-a}^a w(x-y) dy + I(x) = \left[ W(x+a) - W(x-a) + I(x) \right] \quad (4.49)$$

where  $W(x) = \int_0^x w(y) dy$ . The bump halfwidth  $a$  is then determined by requiring (4.49) to satisfy the *threshold conditions*  $U_o(\pm a) = \theta$  which, by even symmetry, result in

$$W(2a) + I(a) = (1 + \beta)\theta. \quad (4.50)$$

This determines the existence of the stationary bump if all assumptions are satisfied. Condition (4.50) was solved numerically in Fig. 4.6 where  $w$  and  $I$  were taken to be

$$w(x) = \frac{\bar{w}_e}{\sqrt{\pi}\sigma_e} e^{-(x/\sigma_e)^2} - \frac{\bar{w}_i}{\sqrt{\pi}\sigma_i} e^{-(x/\sigma_i)^2}, \quad I(x) = I_o e^{-(x/\sigma)^2}. \quad (4.51)$$

### Existence Results for Stationary Bumps for General $w$ and Gaussian-like $I$ .

**CASE I:** *No Input* ( $I(x) = 0$ ). For an excitatory weight function ( $w(x) > 0$ ), stationary bumps exist and satisfy (4.50) when parameters permit ( $0 < \theta < \lim_{x \rightarrow \infty} W(x)$ ); however, they are always linearly unstable [22, 23, 39]. The case of a Mexican hat weight function  $w$  is an extension of the Amari neural field [1] with the existence equation containing an extra factor due to adaptation ( $W(2a) = \theta(1 + \beta)$ ); however, the

dynamics of the adaptation variable  $v$  additionally governs the stability of the stationary bump [22]. In particular, if  $\alpha < \beta$ , stationary bumps are always unstable. Stable bumps in the scalar model of Amari can extend to this model only for  $\alpha > \beta$ , and a stable bump for  $\alpha > \beta$  destabilizes as  $\alpha$  decreases through  $\alpha = \beta$  leading to a drift instability [22] that gives rise to traveling bumps.

**CASE II:** *Localized Excitatory Input* ( $I(x) > 0$ ). A variety of bifurcation scenarios can occur [22, 23], and, importantly, stationary bumps can emerge in a saddle-node bifurcation for strong inputs in parameter regimes where stationary bumps do not exist for weak or zero input as shown in Fig. 4.6. When stationary bumps exist for  $\alpha > \beta$ , the stability of a bump is determined directly by the geometry of the bifurcation curves [22, 23] (e.g., see Fig. 4.6). As  $\alpha$  decreases through  $\alpha = \beta$ , a Hopf bifurcation point emerges from a saddle-node bifurcation point (associated with the sum mode  $\Omega_+$ ) and destabilizes a segment of a branch of stable bumps for  $\alpha < \beta$ . Generally, Hopf bifurcations occur with respect to either of two spatial modes  $\Omega_{\pm}$  (discussed later), and their relative positions (denoted by  $H_{\oplus}$  and  $H_{\ominus}$ , respectively, on the bifurcation curves in Fig. 4.6) can switch depending on parameters [22].

**Stability of Stationary Bumps.** By setting  $u(x, t) = U_o(x, t) + \tilde{\varphi}(x, t)$  and  $v(x, t) = V_o(x, t) + \tilde{\psi}(x, t)$ , we study the evolution of small perturbations  $(\tilde{\varphi}, \tilde{\psi})^T$  in a Taylor expansion of (4.1) about the stationary bump  $(U_o, V_o)^T$ . To first order in  $(\tilde{\varphi}, \tilde{\psi})^T$ , the perturbations are governed by the linearization

$$\begin{aligned} \partial_t \tilde{\varphi} &= -\tilde{\varphi} - \beta \tilde{\psi} + \int_{-\infty}^{\infty} w(x-y) H'(U_o(y) - \theta) \tilde{\varphi}(y, t) dy, \\ \frac{1}{\alpha} \partial_t \tilde{\psi} &= +\tilde{\varphi} - \tilde{\psi}. \end{aligned} \quad (4.52)$$

Separating variables, we set  $\tilde{\varphi}(x, t) = e^{\lambda t} \varphi(x)$  and  $\tilde{\psi}(x, t) = e^{\lambda t} \psi(x)$  in (4.52) where  $(\varphi, \psi)^T \in C_u^1(\mathbb{R}, \mathbb{C}^2)$  denoting uniformly continuously differentiable vector-valued functions  $\mathbf{u} : \mathbb{R} \rightarrow \mathbb{C}^2$ . This leads to the spectral problem for  $\lambda$  and  $(\varphi, \psi)^T$

$$M \begin{pmatrix} \varphi \\ \psi \end{pmatrix} = \lambda \begin{pmatrix} \varphi \\ \psi \end{pmatrix}, \quad M \begin{pmatrix} \varphi \\ \psi \end{pmatrix} = \begin{bmatrix} -1 & -\beta \\ \alpha & -\alpha \end{bmatrix} \begin{pmatrix} \varphi \\ \psi \end{pmatrix} + \begin{pmatrix} \mathcal{N}\varphi \\ 0 \end{pmatrix}, \quad (4.53)$$

where  $\mathcal{N}\varphi(x) = \int_{-\infty}^{\infty} w(x-y) H'(U_o(y) - \theta) \varphi(y) dy$ . The essential spectrum lies in the left-half complex plane and plays no role in instability [22, 23]. To calculate the point spectrum, define  $\rho(\lambda) = \lambda + 1 + \frac{\alpha\beta}{\lambda + \alpha}$  and reduce (4.53) to  $\psi(x) = \left(\frac{\alpha}{\lambda + \alpha}\right)\varphi(x)$  and

$$\rho(\lambda)\varphi(x) = \frac{w(x-a)}{|U_o'(+a)|} \varphi(a) + \frac{w(x+a)}{|U_o'(-a)|} \varphi(-a). \quad (4.54)$$

Setting  $x = \pm a$  in (4.54) yields a compatibility condition for the values of  $\varphi(\pm a)$

$$\left(\Lambda_\circ - \rho(\lambda)\mathbf{I}\right)\begin{pmatrix} \varphi(+a) \\ \varphi(-a) \end{pmatrix} = 0, \quad \Lambda_\circ = \frac{1}{|U'_\circ(a)|} \begin{bmatrix} w(0) & w(2a) \\ w(2a) & w(0) \end{bmatrix}.$$

Consequently, nontrivial solutions of (4.53) exist when  $\det(\Lambda_\circ - \rho(\lambda)\mathbf{I}) = 0$ , thereby identifying eigenvalues  $\lambda$ . The point spectrum comprises two pairs of eigenvalues  $\lambda_\pm^+$ ,  $\lambda_\pm^-$  and eigenfunctions  $\mathbf{v}_\pm^+$ ,  $\mathbf{v}_\pm^-$  defining two characteristic spatial modes [22, 23]:

*Sum mode*: eigenvalues  $\lambda_\pm^+$  and eigenfunctions  $\mathbf{v}_\pm^+(x) = \Omega_+(x)(\lambda_\pm^+ + \alpha, \alpha)^\top$ ,

$$\lambda_\pm^+(a) = -\frac{1}{2}\Upsilon_+ \pm \frac{1}{2}\sqrt{\Upsilon_+^2 - 4\Gamma_+}, \quad \Omega_+(x) = w(x-a) + w(x+a),$$

*Difference Mode*: eigenvalues  $\lambda_\pm^-$  and eigenfunctions  $\mathbf{v}_\pm^-(x) = \Omega_-(x)(\lambda_\pm^- + \alpha, \alpha)^\top$ ,

$$\lambda_\pm^-(a) = -\frac{1}{2}\Upsilon_- \pm \frac{1}{2}\sqrt{\Upsilon_-^2 - 4\Gamma_-}, \quad \Omega_-(x) = w(x-a) - w(x+a),$$

where  $\Omega_+(x)$  is *even*-symmetric,  $\Omega_-(x)$  is *odd*-symmetric, and  $\Upsilon_\pm$ ,  $\Gamma_\pm$  are given by

$$\Upsilon_\pm(a) = 1 + \alpha - \frac{\Omega_\pm(a)}{|U'_\circ(a)|}, \quad \Gamma_\pm(a) = \alpha \left[ 1 + \beta - \frac{\Omega_\pm(a)}{|U'_\circ(a)|} \right].$$

### Stability Results for Stationary Bumps for General $w$ and Gaussian-like $I$ .

**CASE I:** *No Input* ( $I(x) = 0$ ) [22, 23, 25, 41]. Since  $|U'_\circ(a)| = \Omega_-(a)/(1 + \beta)$ ,  $\Gamma_-(a) = 0$  and we can redefine the eigenvalues  $\lambda_\pm^-$  as  $\lambda_+^- \equiv 0$  and  $\lambda_-^- = \beta - \alpha$ . The persistent 0-eigenvalue  $\lambda_+^- \equiv 0$  corresponds to the translation invariance of the stationary bump and is associated with an eigenfunction in the difference mode  $\Omega_-$ . The other eigenfunction in the difference mode (associated with  $\lambda_-^-$ ) is stable for  $\beta < \alpha$  and unstable for  $\alpha < \beta$ . Thus, for  $\alpha < \beta$ , a stationary bump is always linearly unstable. For  $\beta < \alpha$ , a stationary bump can be linearly stable for a Mexican hat weight function (if  $w(2a) < 0$ ) but is always unstable for an excitatory weight function ( $w(x) > 0$ ) [22]. For  $\beta < \alpha$ , it is not possible for a stable stationary bump to undergo a Hopf bifurcation and, as  $\beta$  is increased through  $\alpha$ , a stable stationary bump undergoes a drift instability due to eigenvalue  $\lambda_-^-$  increasing through 0 [22]. Interestingly, a multibump solution in (4.1) on a two-dimensional domain is capable of undergoing a bifurcation to a rotating traveling multibump solution [37].

**CASE II:** *Localized Excitatory Input* ( $I(x) > 0$ ) [7, 22, 23]. The input inhomogeneity ( $I(x) \neq 0$ ) breaks translation symmetry and  $\lambda_+^- \neq 0$  generically. A stationary bump is linearly stable when  $\Re \lambda_\pm^+, \Re \lambda_\pm^- < 0$  which reduce to the conditions

$$\frac{\Omega_+(a)}{|U'_o(a)|} < 1 + \beta \quad \text{if} \quad \alpha > \beta, \quad \frac{\Omega_\pm(a)}{|U'_o(a)|} < 1 + \alpha \quad \text{if} \quad \alpha < \beta.$$

For any stationary bump  $U_o(x)$ , (4.49) implies  $(1 + \beta)|U'_o(a)| = w(0) - w(2a) + |I'(a)|$ . Consequently, the stability conditions translate, in terms of the gradient  $|I'(a)|$ , to

$$\begin{aligned} \alpha > \beta : \quad & |I'(a)| > D_{SN}(a) \equiv 2w(2a), \\ \alpha < \beta : \quad & |I'(a)| > D_H(a) \equiv \begin{cases} \left(\frac{\beta-\alpha}{1+\alpha}\right)\Omega_+(a) + 2w(2a), & w(2a) \geq 0, \\ \left(\frac{\beta-\alpha}{1+\alpha}\right)\Omega_-(a), & w(2a) < 0. \end{cases} \end{aligned}$$

$|I'(a)| = D_{SN}(a)$  denotes a saddle-node bifurcation point and  $|I'(a)| = D_H(a)$  denotes a Hopf bifurcation where a pair of complex eigenvalues associated with one of the two spatial modes  $\Omega_\pm$  crosses into the right-half plane. If  $w(2a) > 0$  at the Hopf bifurcation point, the sum mode  $\Omega_+$  destabilizes and gives rise to a *breather*—a time-periodic, localized bump-like solution that expands and contracts. If  $w(2a) < 0$  at the Hopf bifurcation point, the difference mode  $\Omega_-$  destabilizes and gives rise to a *slosher*—a time-periodic localized solution that instead sloshes side-to-side as shown in Fig. 4.7. Slosers were also found to occur in [26]. Nonlinear analysis of the Hopf bifurcation reveals that, to first order, the breather and slosher are time-periodic modulations of the stationary bump  $U_o(x)$  based upon the even and odd geometry of the sum and difference modes, respectively [22]. The bifurcation can be super/subcritical, which can be determined from the normal form or amplitude equation derived in [22]. Stimulus-induced breathers can undergo further transitions, e.g., period doubling, and can also exhibit mode-locking between breathing and emission of traveling bumps (when supported by the network) [23, 25]. Alternatively, stationary and breathing *fronts* occur in the case of step function input inhomogeneities  $I(x)$  [6, 7]. Hopf bifurcation of radially symmetric stationary bumps extends to (4.1) on two-dimensional domains, leading to a variety of localized time-periodic solutions including nonradially symmetric oscillatory structures [23, 24].

#### 4.4.2 Natural and Stimulus-Locked Traveling Activity Bumps

**Existence of Traveling Bumps.** We simultaneously consider the two cases of *natural* traveling bumps ( $I(x, t) = 0$ ) and *stimulus-locked* traveling bumps which are locked to a stimulus  $I(x, t) = I(x - ct)$  traveling with constant speed  $c$ . Natural traveling bumps in neural field (4.1) on the infinite line  $D = (-\infty, \infty)$  were first considered in [38, 39] and can occur in the absence of an input or in a region of the

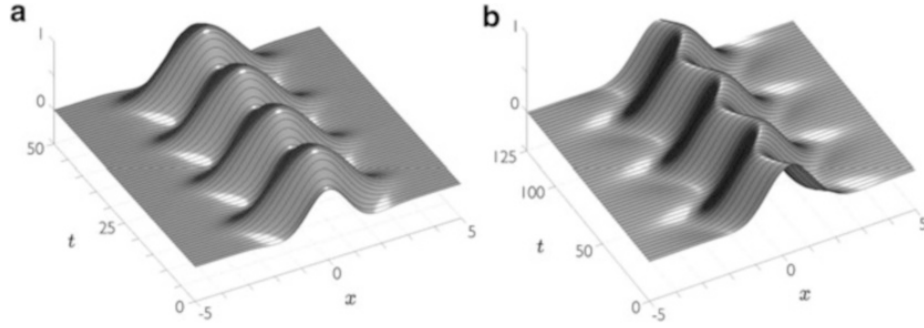


**Fig. 4.7** Destabilization of spatial modes  $\Omega_+(x)$  and  $\Omega_-(x)$ , as the bifurcation parameter  $I_o$  is varied through a Hopf bifurcation, can give rise to a stable *breather* or *slosher*, respectively, depending on the relative position of the bifurcation points for each spatial mode (e.g.,  $H_\oplus$  and  $H_\ominus$ , Fig. 4.6c). **(a)** a plot of  $u(x, t)$  exhibiting a breather arising from destabilization of the sum mode  $\Omega_+(x)$  for  $I_o = 1.9$ ,  $\bar{w}_i = 0$ ,  $\beta = 2.75$ ,  $\alpha = 0.1$ ,  $\theta = 0.375$ . **(b)** a plot of  $u(x, t)$  exhibiting a slosher arising from destabilization of the difference mode  $\Omega_-(x)$  for  $I_o = 1.5$ ,  $\bar{w}_i = 0.4$ ,  $\sigma_i = 2$ ,  $\beta = 2.6$ ,  $\alpha = 0.01$ ,  $\theta = 0.35$ . Common parameters:  $\sigma = 1.2$ ,  $\bar{w}_e = 1$ ,  $\sigma_e = 1$

neural medium where an input is effectively zero [23, 25]. An important distinction between the two cases is that the natural traveling bump in the absence of the input is translationally invariant and we have stability with respect to a family of translates, whereas in the stimulus-locked case there is a fixed position of the bump relative to the input.

Assume  $u(x, t) = U(x - ct)$  and  $v(x, t) = V(x - ct)$  in (4.1) and, in traveling wave coordinates  $\xi = x - ct$ , make the assumption that the activity  $U(\xi)$  is superthreshold  $U(\xi) > \theta$  for  $\xi \in (\xi_1, \xi_2)$ , satisfies  $U(\xi_{1,2}) = \theta$ , and is subthreshold otherwise with  $U(\xi) \rightarrow 0$  as  $\xi \rightarrow \pm\infty$ . Consequently, the profile of the bump satisfies

$$\begin{aligned} -c U_\xi &= -U - \beta V + \int_{-\infty}^{\infty} w(\xi - \eta) H(U(\eta) - \theta) d\eta + I(\xi), \\ -\frac{c}{\alpha} V_\xi &= +U - V. \end{aligned} \quad (4.55)$$

Variation of parameters [25, 55] can be used to solve (4.55) to construct the profile  $(U_c, V_c)^T$  of the traveling bump which can be expressed as [25]

$$\begin{aligned} U_c(\xi) &= (1 - \mu_-) \mathcal{M}_+(\xi) - (1 - \mu_+) \mathcal{M}_-(\xi) \\ V_c(\xi) &= -\alpha [\mathcal{M}_+(\xi) - \mathcal{M}_-(\xi)]. \end{aligned}$$

where  $m(\xi) = W(\xi - \xi_1) - W(\xi - \xi_2) + I(\xi)$ ,

$$\mathcal{M}_\pm(\xi) = \frac{1}{c(\mu_+ - \mu_-)} \int_\xi^\infty e^{\frac{\mu_\pm}{c}(\xi - \eta)} m(\eta) d\eta, \quad \mu_\pm = \frac{1}{2}(1 + \alpha \pm \sqrt{(1 - \alpha)^2 - 4\alpha\beta}),$$

and  $0 < \text{Re } \mu_- \leq \text{Re } \mu_+$ . Since  $m(\xi)$  is dependent upon  $\xi_1, \xi_2$ , the threshold conditions  $U_c(\xi_i) = \theta$ , where  $i = 1, 2$  and  $\xi_1 < \xi_2$ , determine the position of

the two threshold crossings of the bump relative to the position of the input  $I(\xi)$ . This results in consistency conditions for the existence of a *stimulus-locked* traveling bump:

$$\begin{aligned}\theta &= (1 - \mu_-)\mathcal{M}_+(\xi_1) - (1 - \mu_+)\mathcal{M}_-(\xi_1), \\ \theta &= (1 - \mu_-)\mathcal{M}_+(\xi_2) - (1 - \mu_+)\mathcal{M}_-(\xi_2).\end{aligned}$$

These determine the existence of a traveling bump (provided the profile satisfies the assumed threshold conditions) and also include the case of *natural waves* ( $I_o = 0$ ) with the difference being that the conditions instead determine the width  $a = \xi_2 - \xi_1$  of any translate of the bump and its wave speed  $c$  which is selected by the network. Note that existence equations for the traveling bump in (4.55) can also be derived using a second order ODE formulation [23, 39] or an integral formulation [9].

**Existence Conditions for a Positive, Exponential  $w$  and Gaussian  $I$ .** For explicit calculations in this section,  $w$  and  $I$  are taken to be

$$w(x) = \frac{\bar{w}_e}{2\sigma_e} e^{-|x|/\sigma_e}, \quad I(x - ct) = I_o e^{-((x-ct)/\sigma)^2}. \quad (4.56)$$

**CASE I:** *Natural Traveling Bump* ( $I(\xi) = 0$ ) with Speed  $c$  [9, 23, 25, 39, 41]. In the absence of an input, translation invariance of the bump allows the simplification  $(\xi_1, \xi_2) = (0, a)$  where the wave speed  $c$  and bump width  $a$  are naturally selected by the network according to the following threshold conditions [25]

$$\theta = J_+(-a), \quad \theta = K(-a), \quad (4.57)$$

where  $K(\zeta) = J_-(\zeta) - H_+(\zeta) + H_-(\zeta)$ , and, for  $w$  given in (4.56),

$$J_{\pm}(\zeta) = \frac{(\alpha \pm c)(1 - e^{\zeta})}{2(c \pm \mu_+)(c \pm \mu_-)}, \quad H_{\pm}(\zeta) = \frac{c^2(1 - \mu_{\mp})(1 - e^{\frac{\mu_{\pm}}{c}\zeta})}{\mu_{\pm}(c^2 - \mu_{\pm}^2)(\mu_+ - \mu_-)}. \quad (4.58)$$

Note that  $(c \pm \mu_+)(c \pm \mu_-) = c^2 \pm c(1 + \alpha) + \alpha(1 + \beta)$ . Existence equations (4.57) were solved numerically in Fig. 4.8b indicating two branches of traveling bumps for small  $\alpha$ . The wide, faster bump is found to be stable and the narrow, slower bump is unstable.

Detailed analyses of the existence of natural traveling bumps can be found in [41, 52], including the case where the homogeneous state has complex eigenvalues [52]. A singular perturbation construction for the pulse was carried out for smooth firing rate functions  $F$  in [39]. For moderate values of  $\beta$  traveling fronts occur in (4.1) and were shown to undergo a *front bifurcation* in the form of a cusp bifurcation with respect to the wave speed of the front [6].

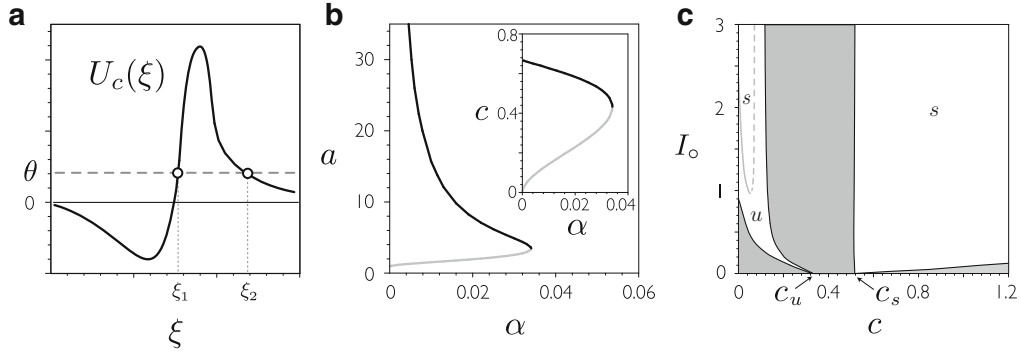


**Fig. 4.8** (a) Traveling bump profile. (b) Bifurcation curves for *natural* traveling bumps ( $I_o = 0$ ) in (4.1) in the  $(\alpha, a)$ -plane and  $(\alpha, c)$ -plane. The stable branch (*black*) of wide, fast bumps and the unstable branch (*gray*) of narrow, slow bumps annihilate in a saddle-node bifurcation at a critical value  $\alpha_c \approx 0.0341$ . (c) Regions of existence (*white*) of the *stimulus-locked* traveling bumps in the  $(c, I_o)$ -plane for fixed  $\sigma = 1, \alpha = 0.03$ . The left and right regions form tongues that issue from the unstable  $c_u$  and stable  $c_s$  natural traveling bumps, respectively. The curve of Hopf bifurcations within the left tongue is shown in *gray*, above which the bump is stable (*s*) and below which it is unstable (*u*). Stable traveling breathers bifurcate from the left branch (*solid gray*) Hopf curve, and stationary bumps correspond to the intersection of the tongue and the line  $c = 0$ . When bumps and breathers are unstable or do not exist, there is mode-locking between breathing and the emission of natural traveling bumps. Parameters in (b) and (c):  $\theta = 0.3, \beta = 2.5, \bar{w}_e = \sigma_e = 1, \bar{w}_i = 0$  (Figure adapted from Folias and Bressloff [25])

**CASE II:** *Stimulus-Locked Traveling Bump* ( $I(\xi) \neq 0$ ) with Speed  $c$  [25]. The wave and stimulus speeds  $c$  are identical, and the threshold conditions for  $(\xi_1, \xi_2)$  are [25]

$$\begin{aligned} \theta &= K(\xi_1 - \xi_2) + T_+(\xi_1) - T_-(\xi_1), \\ \theta &= J_+(\xi_1 - \xi_2) + T_+(\xi_2) - T_-(\xi_2), \end{aligned} \quad (4.59)$$

where  $K, J_+$  are given in (4.58) and  $T_{\pm}$  arises from the input and is given by

$$T_{\pm}(\zeta) = \frac{\sqrt{\pi} \sigma I_o}{2c} \left( \frac{1 - \mu_{\mp}}{\mu_+ - \mu_-} \right) \exp \left( \frac{\mu_{\pm} \zeta}{c} + \left[ \frac{\mu_{\pm} \sigma}{2c} \right]^2 \right) \operatorname{erfc} \left( \frac{\zeta}{\sigma} + \frac{\mu_{\pm} \sigma}{2c} \right),$$

with  $\operatorname{erfc}(z)$  denoting the complementary error function. Equation (4.59) can be solved numerically to determine the regions of existence of stimulus-locked traveling bumps as both the speed  $c$  and amplitude  $I_o$  are varied (assuming  $U_c(\xi)$  satisfies the threshold assumptions). This allows us to connect the stationary bumps to natural traveling bumps via stimulus-locked traveling bumps as shown in Fig. 4.8. This analysis for stimulus-locked fronts was carried out in [6] and an extension of stimulus-locked bumps for a general smooth firing rate function  $F$  was studied in [20].

**Stability of Traveling Bumps.** By setting  $u = U_c + \tilde{\varphi}$  and  $v = V_c + \tilde{\psi}$ , we study the evolution of small perturbations  $(\tilde{\varphi}, \tilde{\psi})^T$  in the linearization of (4.1) about the traveling bump  $(U_c, V_c)^T$  which, in traveling wave coordinates, are governed by

$$\begin{aligned}\partial_t \tilde{\varphi} &= c \partial_\xi \tilde{\varphi} - \tilde{\varphi} - \beta \tilde{\psi} + \int_{-\infty}^{\infty} w(\xi - \eta) H'(U_c(\eta) - \theta) \tilde{\varphi}(\eta, t) d\eta, \\ \partial_t \tilde{\psi} &= c \partial_\xi \tilde{\psi} + \alpha \tilde{\varphi} - \alpha \tilde{\psi}.\end{aligned}\quad (4.60)$$

Separating variables by setting  $\tilde{\varphi}(\xi, t) = e^{\lambda t} \varphi(\xi)$  and  $\tilde{\psi}(\xi, t) = e^{\lambda t} \psi(\xi)$  in (4.60), where  $(\varphi, \psi)^T \in C_u^1(\mathbb{R}, \mathbb{C}^2)$ , leads to the spectral problem for  $\lambda$  and  $(\varphi, \psi)^T$

$$(L + \mathcal{N}) \begin{pmatrix} \varphi \\ \psi \end{pmatrix} = \lambda \begin{pmatrix} \varphi \\ \psi \end{pmatrix} \quad (4.61)$$

where

$$L = c \frac{\partial}{\partial \xi} - \begin{bmatrix} 1 & \beta \\ -\alpha & \alpha \end{bmatrix}, \quad \mathcal{N} \begin{pmatrix} \varphi \\ \psi \end{pmatrix} = \begin{pmatrix} 1 \\ 0 \end{pmatrix} \left[ \frac{w(\xi - \xi_1)}{|U_c'(\xi_1)|} \varphi(\xi_1) + \frac{w(\xi - \xi_2)}{|U_c'(\xi_2)|} \varphi(\xi_2) \right].$$

The essential spectrum lies within the set  $D = \{z : \operatorname{Re} z \in [-\operatorname{Re} \mu_+, -\operatorname{Re} \mu_-]\}$ , where  $\operatorname{Re} \mu_\pm > 0$ , inducing no instability [25, 41, 55]. Stability is then determined by elements of the point spectrum that lie in the region  $R = \{z : \operatorname{Re} z > -\operatorname{Re} \mu_-\}$  which can be calculated using an Evans function. In particular, we determine a condition for  $(L + \mathcal{N} - \lambda I)$  to have a bounded inverse. The Evans function  $\mathcal{E}(\lambda)$  subsequently arises from the condition that  $(L + \mathcal{N} - \lambda I)$  is not invertible and  $(L + \mathcal{N} - \lambda I) \mathbf{u} = 0$  has nontrivial solutions. We set  $\mathbf{u} = (\varphi, \psi)^T$  and use variation of parameters [25, 55] to construct a bounded inverse for  $(L + \mathcal{N} - \lambda I)$  based on the integral kernel

$$\mathbf{M}(\xi, \eta, \lambda) = \frac{1}{c\beta(\mu_+ - \mu_-)} \left[ \Phi_+(\xi) | \Phi_-(\xi) \right] \left[ \Psi_+(\eta) | \Psi_-(\eta) \right]^T \quad (4.62)$$

where  $[A|B]$  denotes the matrix with column vectors A and B, respectively, and

$$\Phi_\pm(\xi) = \begin{pmatrix} \beta \\ \mu_\pm - 1 \end{pmatrix} e^{(\frac{\lambda + \mu_\pm}{c})\xi}, \quad \Psi_\pm(\xi) = \pm \begin{pmatrix} 1 - \mu_\mp \\ \beta \end{pmatrix} e^{-\frac{(\lambda + \mu_\pm)}{c}\xi}.$$

For  $\operatorname{Re}(\lambda) > -\mu_-$ , we can express  $(L + \mathcal{N} - \lambda I)\mathbf{u} = -\mathbf{f}$ , where  $\mathbf{f} = (f_1, f_2)^T$ , as

$$\mathbf{u}(\xi) - \int_\xi^\infty \mathbf{M}(\xi, \eta, \lambda) \mathcal{N} \mathbf{u}(\eta) d\eta = \int_\xi^\infty \mathbf{M}(\xi, \eta, \lambda) \mathbf{f}(\eta) d\eta. \quad (4.63)$$

From (4.63),  $\psi$  is calculated in terms of  $\varphi(\xi_1)$ ,  $\varphi(\xi_2)$ ,  $\mathcal{F}_2$ , and  $\lambda, \varphi$  are determined by

$$\varphi(\xi) - \Lambda_1(\lambda, \xi)\varphi(\xi_1) - \Lambda_2(\lambda, \xi)\varphi(\xi_2) = \mathcal{F}_1(\xi) \quad (4.64)$$

where  $M_{11}$  denotes the  $(1,1)$  entry of  $M$  in (4.62) and  $i = 1, 2$  in the expression below

$$\Lambda_i(\lambda, \xi) = \int_{\xi}^{\infty} M_{11}(\xi, \eta, \lambda) \frac{w(\eta - \xi_i)}{|U'_c(\xi_i)|} d\eta, \quad \begin{pmatrix} \mathcal{F}_1(\xi) \\ \mathcal{F}_2(\xi) \end{pmatrix} = \int_{\xi}^{\infty} M(\xi, \eta, \lambda) \mathbf{f}(\eta) d\eta.$$

By the Hölder inequality,  $\Lambda_i$  and  $\mathcal{F}_{1,2}$  are bounded for all  $\xi \in \mathbb{R}$  and  $\mathbf{f} \in C_u^0(\mathbb{R}, \mathbb{C}^2)$ . A compatibility condition that determines the values of  $\varphi(\xi_1)$  and  $\varphi(\xi_2)$  is produced by substituting  $\xi = \xi_1$  and  $\xi = \xi_2$  into (4.64) to obtain the matrix equation

$$\left( \mathbf{I} - \Lambda(\lambda) \right) \begin{pmatrix} \varphi(\xi_1) \\ \varphi(\xi_2) \end{pmatrix} = \begin{pmatrix} \mathcal{F}_1(\xi_1) \\ \mathcal{F}_1(\xi_2) \end{pmatrix}, \quad \Lambda(\lambda) = \begin{bmatrix} \Lambda_1(\lambda, \xi_1) & \Lambda_2(\lambda, \xi_1) \\ \Lambda_1(\lambda, \xi_2) & \Lambda_2(\lambda, \xi_2) \end{bmatrix}$$

which has a unique solution if and only if  $\det(\mathbf{I} - \Lambda(\lambda)) \neq 0$ , resulting in a bounded inverse  $(L + N - \lambda \mathbf{I})^{-1}$  defined on all of  $C_u^0(\mathbb{R}, \mathbb{C}^2)$ . Conversely, we cannot invert the operator for  $\lambda$  such that  $\det(\mathbf{I} - \Lambda(\lambda)) = 0$ , in which case  $(L + N - \lambda)\mathbf{u} = \mathbf{0}$  has nontrivial solutions corresponding to eigenvalues  $\lambda$  and eigenfunctions  $(\varphi, \psi)^T$  in the point spectrum. Thus, for  $\operatorname{Re}(\lambda) > -\mu_-$ , we can express the *Evans function* as

$$\mathcal{E}(\lambda) = \det(\mathbf{I} - \Lambda(\lambda)), \quad \operatorname{Re}(\lambda) > -\mu_-, \quad (4.65)$$

which has eigenvalues  $\lambda$  given by its zero set.

**Evans Function for an Exponential Weight  $w$  and Gaussian-like Input  $I$ .** The following gives an explicit construction of the Evans function for natural ( $I_o = 0$ ) and stimulus-locked ( $I_o > 0$ ) traveling bumps in (4.1) with a Heaviside firing rate function, exponential weight distribution and Gaussian input given in (4.56). For natural traveling bumps ( $I_o = 0$ ), by translation invariance we set  $(\xi_1, \xi_2) = (0, a)$ .

For  $\operatorname{Re}(\lambda) > -\mu_-$ , the Evans function  $\mathcal{E}(\lambda)$  is given by [25]

$$\mathcal{E}(\lambda) = \left[ 1 - \frac{\Theta_+(\lambda)}{|U'_c(\xi_1)|} \right] \left[ 1 - \frac{\Theta_+(\lambda)}{|U'_c(\xi_2)|} \right] - \frac{\Theta_+(\lambda) \mathcal{E}(\lambda, \xi_1 - \xi_2)}{|U'_c(\xi_1)U'_c(\xi_2)|},$$

where

$$\Gamma_{\pm}(\lambda) = \frac{(1 - \mu_{\mp})c}{(\mu_+ - \mu_-)(c^2 - (\lambda + \mu_{\pm})^2)}, \quad \Theta_{\pm}(\lambda) = \frac{\lambda + \alpha \pm c}{2(\lambda + \mu_+ \pm c)(\lambda + \mu_- \pm c)},$$

$$\mathcal{E}(\lambda, \xi) = \Theta_-(\lambda)e^{2\xi} + \Gamma_+(\lambda)e^{\left[\frac{\lambda + \mu_+ + c}{c}\right]\xi} - \Gamma_-(\lambda)e^{\left[\frac{\lambda + \mu_- + c}{c}\right]\xi}.$$

Since the zero set of the Evans function  $\mathcal{E}(\lambda)$  comprises solutions of a transcendental equation, the eigenvalues  $\lambda$  can be determined numerically by finding the intersection points of the zero sets of the real and imaginary parts of the Evans function which was used to determine the stability results in Fig. 4.8. Hopf bifurcations, identified by complex conjugate eigenvalues crossing the imaginary axis, can give rise to traveling breathers or mode-locking between breathing and the emission of natural traveling bumps [25].

For various treatments of the stability of natural traveling bumps and Evans functions in (4.1) see [4, 10, 25, 41, 44, 55], and a comparison between different approaches is found in [44]. Zhang developed the Evans function and analyzed the stability of traveling bumps in the singularly perturbed case  $0 < \alpha \ll 1$  [55]. Finally, on one-dimensional domains, traveling multibump waves were studied in [52], and traveling waves have been extended to the case of inhomogeneous synaptic coupling in [32] and asymmetric coupling [51]. On two-dimensional domains, circular waves/target patterns [23], spiral waves [34, 52], traveling and rotating multibumps [37], and the collision of traveling bumps [36] have also been examined.

## References

1. Amari, S.: Dynamics of pattern formation in lateral-inhibition type neural fields. *Biol. Cybern.* **27**(2), 77–87 (1977)
2. Benda, J., Herz, A.V.M.: A universal model for spike-frequency adaptation. *Neural Comput.* **15**(11), 2523–2564 (2003)
3. Billock, V.A., Tsou, B.H.: Elementary visual hallucinations and their relationships to neural pattern-forming mechanisms. *Psychol. Bull.* **138**(4), 744–774 (2012)
4. Bressloff, P.C.: Spatiotemporal dynamics of continuum neural fields. *J. Phys. A: Math. Theor.* **45**(3), 033,001 (2012)
5. Bressloff, P.C., Cowan, J.D., Golubitsky, M., Thomas, P.J., Wiener, M.C.: Geometric visual hallucinations, Euclidean symmetry and the functional architecture of striate cortex. *Philos. Trans. R. Soc. B.* **356**(1407), 299–330 (2001)
6. Bressloff, P.C., Folias, S.E.: Front bifurcations in an excitatory neural network. *SIAM J. Appl. Math.* **65**, 131–151 (2004)
7. Bressloff, P.C., Folias, S.E., Prat, A., Li, Y.X.: Oscillatory waves in inhomogeneous neural media. *Phys. Rev. Lett.* **91**(17), 178,101 (2003)
8. Coombes, S.: Waves, bumps, and patterns in neural field theories. *Biol. Cybern.* **93**(2), 91–108 (2005)
9. Coombes, S., Lord, G.J., Owen, M.R.: Waves and bumps in neuronal networks with axo-dendritic synaptic interactions. *Phys. D* **178**, 219–241 (2003)
10. Coombes, S., Owen, M.R.: Evans functions for integral neural field equations with Heaviside firing rate function. *SIAM J. Appl. Dyn. Syst.* **3**(4), 574–600 (2004)
11. Coombes, S., Owen, M.R.: Bumps, breathers, and waves in a neural network with spike frequency adaptation. *Phys. Rev. Lett.* **94**(14), 148,102 (2005)
12. Coombes, S., Schmidt, H., Bojak, I.: Interface dynamics in planar neural field models. *J. Math. Neurosci.* **2**, 9 (2012)
13. Curtu, R., Ermentrout, B.: Pattern formation in a network of excitatory and inhibitory cells with adaptation. *SIAM J. Appl. Dyn. Syst.* **3**, 191–231 (2004)
14. Dawes, J.H.P.: Hopf bifurcation on a square superlattice. *Nonlinearity* **14**, 491 (2001)

15. Dionne, B., Silber, M., Skeldon, A.C.: Stability results for steady, spatially periodic planforms. *Nonlinearity* **10**, 321 (1997)
16. Ermentrout, B.: Stripes or spots? Nonlinear effects in bifurcation of reaction-diffusion equations on the square. *Proc. R. Soc. Lond. Ser. A: Math. Phys. Sci.* **434**(1891), 413–417 (1991)
17. Ermentrout, B.: Neural networks as spatio-temporal pattern-forming systems. *Rep. Prog. Phys.* **61**, 353–430 (1998)
18. Ermentrout, G.B., Cowan, J.D.: A mathematical theory of visual hallucination patterns. *Biol. Cybern.* **34**(3), 137–150 (1979)
19. Ermentrout, G.B., Cowan, J.D.: Secondary bifurcation in neuronal nets. *SIAM J. Appl. Math.* **39**(2), 323–340 (1980)
20. Ermentrout, G.B., Jalics, J.Z., Rubin, J.E.: Stimulus-driven traveling solutions in continuum neuronal models with a general smooth firing rate function. *SIAM J. Appl. Math.* **70**(8), 3039–3064 (2010)
21. Ermentrout, G.B., McLeod, J.B.: Existence and uniqueness of travelling waves for a neural network. *Proc. R. Soc. Edinb.* **123A**, 461–478 (1993)
22. Folias, S.E.: Nonlinear analysis of breathing pulses in a synaptically coupled neural network. *SIAM J. Appl. Dyn. Syst.* **10**, 744–787 (2011)
23. Folias, S.E., Bressloff, P.C.: Breathing pulses in an excitatory neural network. *SIAM J. Appl. Dyn. Syst.* **3**(3), 378–407 (2004)
24. Folias, S.E., Bressloff, P.C.: Breathers in two-dimensional neural media. *Phys. Rev. Lett.* **95**(20), 208,107 (2005)
25. Folias, S.E., Bressloff, P.C.: Stimulus-locked traveling waves and breathers in an excitatory neural network. *SIAM J. Appl. Math.* **65**(6), 2067–2092 (2005)
26. Hansel, D., Sompolinsky, H.: Modeling feature selectivity in local cortical circuits. In: Koch, C., Segev, I. (eds.) *Methods in Neuronal Modeling: From Ions to Networks*, Chap. 13, pp. 499–567. MIT, Cambridge (1998)
27. Huang, X., Troy, W.C., Yang, Q., Ma, H., Laing, C.R., Schiff, S.J., Wu, J.Y.: Spiral waves in disinhibited mammalian neocortex. *J. Neurosci.* **24**(44), 9897–9902 (2004)
28. Itskov, V., Curto, C., Pastalkova, E., Buzsáki, G.: Cell assembly sequences arising from spike threshold adaptation keep track of time in the hippocampus. *J. Neurosci.* **31**(8), 2828–2834 (2011)
29. Kilpatrick, Z.P., Bressloff, P.C.: Stability of bumps in piecewise smooth neural fields with nonlinear adaptation. *Phys. D* **239**(12), 1048–1060 (2010)
30. Kilpatrick, Z.P., Ermentrout, B.: Wandering bumps in stochastic neural fields. *arXiv (nlin.PS/1205.3072v1)* (2012)
31. Kilpatrick, Z.P., Ermentrout, G.B.: Hallucinogen persisting perception disorder in neuronal networks with adaptation. *J. Comput. Neurosci.* **32**(1), 25–53 (2012)
32. Kilpatrick, Z.P., Folias, S.E., Bressloff, P.C.: Traveling pulses and wave propagation failure in inhomogeneous neural media. *SIAM J. Appl. Dyn. Syst.* **7**(1), 161–185 (2008)
33. Klüver, H.: *Mescal and the Mechanisms of Hallucinations*. University of Chicago Press, Chicago (1966)
34. Laing, C.R.: Spiral waves in nonlocal equations. *SIAM J. Appl. Dyn. Syst.* **4**(3), 588–606 (2005)
35. Laing, C.R., Longtin, A.: Noise-induced stabilization of bumps in systems with long-range spatial coupling. *Phys. D* **160**(3–4), 149–172 (2001)
36. Lu, Y., Sato, Y., Amari, S.I.: Traveling bumps and their collisions in a two-dimensional neural field. *Neural Comput.* **23**(5), 1248–60 (2011)
37. Owen, M.R., Laing, C.R., Coombes, S.: Bumps and rings in a two-dimensional neural field: splitting and rotational instabilities. *New J. Phys.* **9**, 378 (2007)
38. Pinto, D.J.: Computational, experimental, and analytical explorations of neuronal circuits in the cerebral cortex. Ph.D. thesis, Department of Mathematics, University of Pittsburgh, Pittsburgh (1997)
39. Pinto, D.J., Ermentrout, G.B.: Spatially structured activity in synaptically coupled neuronal networks: I. Traveling fronts and pulses. *SIAM J. Appl. Math.* **62**(1), 206–225 (2001)

40. Pinto, D.J., Ermentrout, G.B.: Spatially structured activity in synaptically coupled neuronal networks: II. Lateral inhibition and standing pulses. *SIAM J. Appl. Math.* **62**(1), 226–243 (2001)
41. Pinto, D.J., Jackson, R.K., Wayne, C.E.: Existence and stability of traveling pulses in a continuous neuronal network. *SIAM J. Appl. Dyn. Syst.* **4**, 954–984 (2005)
42. Rankin, J., Tlapale, E., Veltz, R., Faugeras, O., Kornprobst, P.: Bifurcation analysis applied to a model of motion integration with a multistable stimulus. Inria: Research report (2011)
43. Rule, M., Stoffregen, M., Ermentrout, B.: A model for the origin and properties of flicker-induced geometric phosphenes. *PLoS Comput. Biol.* **7**(9), e1002158 (2011)
44. Sandstede, B.: Evans functions and nonlinear stability of traveling waves in neuronal network models. *Int. J. Bifur. Chaos Appl. Sci. Eng.* **17**, 2693–2704 (2007)
45. Schwartz, E.: Spatial mapping in the primate sensory projection: analytic structure and relevance to projection. *Biol. Cybern.* **25**, 181–194 (1977)
46. Shusterman, V., Troy, W.C.: From baseline to epileptiform activity: a path to synchronized rhythmicity in large-scale neural networks. *Phys. Rev. E* **77**(6), 061911 (2008)
47. Silber, M., Knobloch, E.: Hopf bifurcation on a square lattice. *Nonlinearity* **4**, 1063 (1991)
48. Stocker, M., Krause, M., Pedarzani, P.: An apamin-sensitive  $\text{Ca}^{2+}$ -activated  $\text{K}^{+}$  current in hippocampal pyramidal neurons. *Proc. Natl. Acad. Sci. USA* **96**(8), 4662–4667 (1999)
49. Tass, P.: Cortical pattern formation during visual hallucinations. *J. Biol. Phys.* **21**(3), 177–210 (1995)
50. Tass, P.: Oscillatory cortical activity during visual hallucinations. *J. Biol. Phys.* **23**(1), 21–66 (1997)
51. Troy, W.C.: Traveling waves and synchrony in an excitable large-scale neuronal network with asymmetric connections. *SIAM J. Appl. Dyn. Syst.* **7**(4), 1247–1282 (2008)
52. Troy, W.C., Shusterman, V.: Patterns and features of families of traveling waves in large-scale neuronal networks. *SIAM J. Appl. Dyn. Syst.* **6**(1), 263–292 (2007)
53. Wu, J.Y.: Propagating waves of activity in the neocortex: what they are, what they do. *Neuroscientist* **14**(5), 487–502 (2008)
54. Zhang, K.: Representation of spatial orientation by the intrinsic dynamics of the head-direction cell ensemble: a theory. *J. Neurosci.* **16**(6), 2112–2126 (1996)
55. Zhang, L.: On stability of traveling wave solutions in synaptically coupled neuronal networks. *Differ. Integral Equ.* **16**, 513–536 (2003)
56. Zhang, L.: Existence, uniqueness and exponential stability of traveling wave solutions of some integral differential equations arising from neuronal networks. *J. Differ. Equ.* **197**(1), 162–196 (2004)